NAVAL AIR WARFARE CENTER AIRCRAFT DIVISION
PATUXENT RIVER, MARYLAND

TECHNICAL INFORMATION MEMORANDUM

REPORT NO: NAWCADPAX/TIM-2014/26

EFFECT OF YAW ANGLE AND AMBIENT WIND ON FABRIC PENETRATION OF A SIMULATED SLEEVE

by

Mr. Terence A. Ghee
Dr. Suresh Dhaniyala
Mr. Kenneth L. Murphy

August 20, 2015

DEPARTMENT OF THE NAVY
NAVAL AIR WARFARE CENTER AIRCRAFT DIVISION
PATUXENT RIVER, MARYLAND

NAWCADPAX/TIM-2014/26
August 20, 2015

EFFECT OF YAW ANGLE AND AMBIENT WIND ON FABRIC PENETRATION OF A SIMULATED SLEEVE

by

Mr. Terence A. Ghee
Dr. Suresh Dhaniyala
Mr. Kenneth L. Murphy

RELEASED BY:

Steven A. Donaldson August 20, 2015

STEVE DONALDSON / AIR- 4.3.2 / DATE
Head, Aeromechanics Division
Naval Air Warfare Center Aircraft Division

REPORT DOCUMENTATION PAGE

Form Approved
OMB No. 0704-0188

1. REPORT DATE	2. REPORT TYPE	3. DATES COVERED
August 20, 2015	Technical Report	March 2004 – October 2013

4. TITLE AND SUBTITLE

Effect of Yaw Angle and Ambient Wind on Fabric Penetration of a Simulated Sleeve

5a. CONTRACT NUMBER

5b. GRANT NUMBER

5c. PROGRAM ELEMENT NUMBER

6. AUTHOR(S)

Mr. Terence A. Ghee
Dr. Suresh Dhaniyala
Mr. Kenneth L. Murphy

5d. PROJECT NUMBER

5e. TASK NUMBER

5f. WORK UNIT NUMBER

7. PERFORMING ORGANIZATION NAME(S) AND ADDRESS(ES)

Naval Air Warfare Center Aircraft Division
22347 Cedar Point Road,
Patuxent River, Maryland 20670-1161

8. PERFORMING ORGANIZATION REPORT NUMBER

NAWCADPAX/TR-2014/26

9. SPONSORING/MONITORING AGENCY NAME(S) AND ADDRESS(ES)

Naval Air Systems Command
47123 Buse Road
Patuxent River, Maryland 20670-1547

10. SPONSOR/MONITOR'S ACRONYM(S)

11. SPONSOR/MONITOR'S REPORT NUMBER(S)

12. DISTRIBUTION/AVAILABILITY STATEMENT

Approved for public release; distribution is unlimited.

13. SUPPLEMENTARY NOTES

14. ABSTRACT

As part of a program to develop a systematic method to test and quantify Individual Protective Equipment effectiveness, a methodology was developed to test component (sleeve) specimens at elevated wind speeds in the Naval Aerodynamic Test Facility wind tunnel. Tests were conducted to determine the azimuthal pressure characteristics of a circular cylinder with a simulated fabric sleeve. A support screen was placed between the fabric and the circular cylinder to create an idealized flow condition with a constant air gap. With the constrained sleeve, the pressure coefficient around the model inner core was measured and found to be nearly invariant with azimuth and wind velocity and had a value of approximately -0.5. Fabric pressure drop was measured as a variation with model azimuth and found to exhibit a net inflow for angles less than 30 . Above this value the pressure was positive indicating a net outflow. Particle penetration was measured for three yaw angles and at four wind speeds. In general the maximum particle penetration was found to increase with increasing wind velocity and decrease with increasing yaw angle. The results were found to be consistent and repeatable.

Fabric pressure differential/fabric face velocity was found to be a parameter, but not the sole parameter, to quantify particle penetration performance. Further research or analysis may be needed quantify this complex phenomenon completely.

15. SUBJECT TERMS

16. SECURITY CLASSIFICATION OF:			17. LIMITATION OF ABSTRACT	18. NUMBER OF PAGES	19a. NAME OF RESPONSIBLE PERSON
a. REPORT	b. ABSTRACT	c. THIS PAGE			Terence A. Ghee
unclassified	unclassified	unclassified	SAR	57	19b. TELEPHONE NUMBER (include area code) 301-342-8536

Standard Form 298 (Rev 8-98)
Prescribed by ANSI Std Z39-18

SUMMARY

As part of a program to develop a systematic method to test and quantify Individual Protective Equipment effectiveness, a methodology was developed to test component (sleeve) specimens at elevated wind speeds in the Naval Aerodynamic Test Facility wind tunnel. Tests were conducted to determine the azimuthal pressure characteristics of a circular cylinder with a simulated fabric sleeve. A support screen was placed between the fabric and the circular cylinder to create an idealized flow condition with a constant air gap. With the constrained sleeve, the pressure coefficient around the model inner core was measured and found to be nearly invariant with azimuth and wind velocity and had a value of approximately -0.5. Fabric pressure drop was measured as a variation with model azimuth and found to exhibit a net inflow for angles less than 30 deg. Above this value, the pressure was positive indicating a net outflow. Particle penetration was measured for three yaw angles and at four wind speeds. In general, the maximum particle penetration was found to increase with increasing wind velocity and decrease with increasing yaw angle. The results were found to be consistent and repeatable.

Fabric pressure differential/fabric face velocity was found to be a parameter, but not the sole parameter, to quantify particle penetration performance. Further research or analysis may be needed quantify this complex phenomenon completely.

Contents

ACKNOWLEDGEMENTS

The authors wish to thank the Office of Naval Research for providing funding for this work through the Naval Innovative Science and Engineering program (Section 219). In addition, we acknowledge the invaluable support of Mr. Rod Pursell, Ms. Wendy Todd, Mr. Jackson Shannon, and Mr. Christian Egbert.

NOMENCLATURE

A	Effective swatch area, 9.6 cm^2
b	Span length, 0.6096 m
Dp	Particle diameter, nm
N	Number concentration
P	Pressure, mbar
P_∞	Tunnel static pressure, mbar
ΔP	Static pressure difference, mbar
P	Fabric penetration, %
q_∞	Tunnel dynamic pressure, mbar
Q	Volumetric flow rate, Standard Liter per Minute
R	Cylinder radius, 0.1143 m
ΔR	Fabric gap, 0.0159 m
U_o	Fabric face velocity, cm/sec
V_∞	Tunnel freestream velocity, m/sec
w	Permeability, cm/sec
y	Spanwise location, m
α	Fabric permeability, m/sec
ρ	Density, g/ml
μ	Gas constant, 1.7894 X 10^{-5} kg/(m)(sec)
Θ	Azimuth Angle, deg
Ψ	Yaw Angle, deg

INTRODUCTION

Complete isolation from a chemically or biologically contaminated environment provides the best protection against percutaneous effects. This has been the goal of many individual protective equipment (IPE) designs; current ensembles intended to protect users against exposure to high chemical-biological (CB) agent concentrations (e.g., U.S. Marine Corps Chemical Biological Incident Response Force Level A chemical protective overgarment) achieves this isolation by sealing users in a chemically impermeable garment. With this approach, however, heat stress becomes a major problem as normal physiological heat loss mechanisms (especially sweat evaporation) are blocked. Air-permeable materials with treated activated carbon were introduced to mitigate the heat stress problem without compromising CB protection.

The flowrate through air-permeable materials results from pressure differentials between the inside and outside of the garment. These pressure differentials are induced by body motions, e.g., the well-known "bellows effect", c.f., references 1 and 2, as well as by wind. The wind can be the actual outdoor wind, an artificial wind created by helicopter downwash, or a relative wind created by riding on a moving vehicle.

Previous evidence, reference 3, suggested that maintaining IPE protection levels becomes a problem with elevated wind speeds (e.g., some swatch tests show up to 300X increases in IPE penetration with a 3X increase in wind speed). Generally, experiments with swatch, component, and system setups show elevated wind speed increases penetration but did not uniformly indicate the problem is of the same order of magnitude.

Moreover, these results were controversial because much of the data is derived from test methodology that is largely not validated for assessing the effects of elevated wind speeds. For example, data obtained from the Aerosol/Vapor/Liquid Assessment Group swatch test exceed the design parameters of the test cell (i.e., design nominal equivalent wind speed of 3.6 m/sec).

A limited understanding of system-level (full garment) high wind issues based on a lack of high wind speed penetration and deposition studies, combined with combined un-validated test technology to study this issue, has become increasingly relevant as IPE requirements begin to address high wind-associated penetration. The present project was designed to investigate swatch and component tests in the presence of high winds (up to 36.6 m/sec, i.e. 120 ft/sec or 81.8 mph). This paper describes the development of test methodology and results for component (sleeve) testing of fabric material in the wind tunnel at various component yaw angles.

THIS PAGE INTENTIONALLY LEFT BLANK

EXPERIMENTAL APPARATUS

WIND TUNNEL

The tests were conducted in the Naval Aerodynamic Test Facility (NATF) wind tunnel located at Patuxent River, MD reference 4 describes the NATF. The NATF is a 1.22 m by 1.22 m by 2.44 m long (4 ft by 4 ft by 8 ft long) closed test section, open-return wind tunnel, see Figures A-1 and A-2. The facility incorporates a 200 horsepower motor that drives a variable pitch, variable RPM fan and delivers a maximum velocity of 60.96 m/sec (205 ft/s or 140 mph) at the test section. In addition, the facility has honeycomb and three sets of flow conditioning screens that minimize free stream turbulence intensity to approximately 0.5% and free stream velocity differences to 1%.

AEROSOL CHALLENGE

In this study, DiOctyl Sebacate (DOS) manufactured by Sigma-Aldrich (St. Louis, MO) was used as the challenge aerosol material. DOS is a plasticizer that is liquid at room temperature and has a density of 0.914 g/mL.

DISSEMINATION SYSTEM

Common wind tunnel aerosol dissemination is made using an array of tubing with ejectors (usually in the tunnel contraction or settling chamber) that allow dissemination across the wind tunnel cross section. This method proved to be unattractive for use in the NATF. The open-return design of the tunnel—while allowing constant temperature operation through heat exchange with the building heating, ventilation, and air conditioning (HVAC) system—requires continuous dissemination. However, due to the large amount of air volume moved through the wind tunnel, 4785.5 m^3/min (169,000 CFM) at the highest envisioned testing velocity of 53.6 m/sec, it was impractical to disseminate seeding over the entire test section. The facility HVAC system is not a separate system from the rest of the large office building and complaints regarding the adverse effects of the seeding particles are a concern (as are concerns regarding adverse effects on wind tunnel personnel). Also, an array of ejectors downstream of the flow conditioning screens would adversely affect wind tunnel flow quality. Low and high free-stream turbulence levels are of interest to insure that the test methodology is robust enough for use in other facilities: low turbulence flow would be compromised by ejectors in the wind tunnel contraction section. Finally, the facility is principally an aerodynamic research facility with delicate and expensive instrumentation: the seeding must not harm other equipment. These design considerations led to adopting localized seeding of the wind tunnel cross section. The localized seeding method has the added potential benefit of being portable from one facility to another. This mitigates one design variable in conducting the experiments in different facilities.

The system utilized an atomizing nozzle (Spray Systems, Co., Wheaton, Illinois, 1/4JAUMCO-316SS2050) that was installed in a 2.5-gal pressure tank (W.R. Brown Co., North Chicago, Illinois, Model Speed). An earth-grounded, 5-gal pressure tank held a mixture of 200-proof ethanol and 10% DOS. The tank was generally set to 6 psi and pressurized using clean, dry

Nitrogen to avoid challenge contamination. HEPA-filtered shop air supplied the atomizing-nozzle and needle valve and was controlled by a solenoid valve (Skinner Valve, New Britain, Connecticut, 7131T). A schematic of the dissemination system is depicted in Figure A-3 and an image of the system is shown in Figure A-4.

The atomized spray was sent through a custom-made dryer/conditioner which consisted of a capped, clear, 10.2 cm (4 in.) OD PVC pipe, within which a porous metal tube (Mott Corp., Farmington, Connecticut, 1.9 cm (3/4 in. ID) was immersed in a bed of silica beads. The dryer/conditioner eliminated water vapor and most of the ethanol evidenced by a pre-drying peak centered at 50 nm. Downstream of the dryer/conditioner, the peak of the generated particles was at 200 nm. As will be shown in subsequent sections, this arrangement was found to give temporally and spatially repeatable dissemination.

A series of vents were placed between the dryer stage and the dissemination head to reduce the particle concentration to acceptable levels. The vents were filtered using Pall Corporation Model 12144 filters. Finally, the challenge was ejected in the wind tunnel via a series of ¼ in. tubing arranged in a square pattern and oriented facing forward to assist in mixing, see Figure A-5.

INSTRUMENTATION

A TSI (TSI, Inc., St. Paul, MN) Model 3936 Scanning Mobility Particle Sizer (SMPS) was used to acquire particle count, size, and concentration data for sub-micron particles. This unit is composed of a TSI Model 3080 Electrostatic Classifier (with a long differential mobility analyzer) and a TSI Model 3025A Ultrafine Condensation Particle Counter. A 0.0457 cm impactor nozzle was used with an aerosol flow rate of 0.3 liters/minute (l pm) and a sheath flow rate of 3.0l pm to insure a 1-to-10 ratio as recommended by the manufacturer. Larger particles were measured using a TSI Model 3320 Aerodynamic Particle Sizer (APS). The APS had a sheath flow rate of 4.0 l pm and an aerosol flow of 1.0 l pm. The various instrument settings are provided in Appendix B-1.

A Sierra Instruments, Inc. (Monterey, CA) Model C100M Mass Flow Controller was used to control the mass flow rate from a shop air source in order to provide make up air. The additional air flow was controlled such that the total flow (SMPS flow, APS flow, and make-up air) provided the necessary sampling flow rate for each instrument.

Figures A-6 shows a schematic diagram of the instrumentation set up and an image of the instrumentation is seen in Figure A-7.

Basic fabric characteristics were determined via a bench top swatch testing system prior to wind tunnel testing. The pressure differential across a 47mm swatch was measured from bench top experiments using a digital pressure gage (Mensor Corp. San Marcos, Texas, Model 2101). This pressure differential provided a correlation between the wind tunnel sleeve face velocity and the bench top swatch face velocity as determined from a technique developed by NAVAIR and reported in reference 5. A mass flow controller was used to determine permeability and fabric

face velocity variation with differential pressure. Reference 6 describes the bench top set up in greater detail.

Component (sleeve) pressure was measured by a 10-in.-of-water and a 20-in.-of-water electronically-scanned pressure module connected to a Pressure Systems, Inc. (now Measurement Specialties, Inc.) Initium pressure data acquisition system.

SLEEVE MATERIAL

Unless otherwise noted, the material used in the present report was a 2/1 right-hand, 100% cotton twill (denim) weighing 10 oz per square yard purchased from JoAnn Fabrics on 21 May 2010. This material will be referred to as "10 oz. Denim" in the report.

Additional material tested: two commercial filter bags manufactured by Donaldson Company, Inc. (Dura-Life and Tetratex (PTFE)), Kimberly-Clark Corp. Kleenguard A30 Breathable Coveralls, and a commercial cotton twill fabric obtained from JoAnn Fabrics. The material was sewn in-house to form a sleeve that fit snugly over the Component Model.

COMPONENT (SLEEVE) MODEL

A component sleeve fixture was manufactured by Advanced Technologies, Inc. (ATI, Newport News, Virginia) to hold a simulated sleeve in the wind tunnel. The mounting hardware was built by the machine shop at Clarkson University. The 0.6096 m (2 ft) long component sleeve fixture consists of a 0.1143 m (4.5 in.) diameter cylindrical sleeve (with support screen) surrounding a solid inner cylinder (0.0826 m diameter, 3.25 in.), roughly the diameter of a human arm, with a 0.0159 m (0.625 in.) gap between sleeve and inner cylinder (the gap is 0.01429 m (0.5625 in. without support screen). A dummy upper mounting adaptor was installed to minimize flow angularity effects. As seen in Figure A-8a, a support screen was installed to prevent fabric flapping and deformation. A chordwise ring of 22 pressure taps were located 15.88 mm (5/8 in.) above the mid-point of the inner core of the model. Six pressure taps, spanning 0.3048 m (1 ft), were located at 0 deg to the wind to monitor two-dimensional flow. To measure the pressure drop across the fabric of the constrained sleeve (Figure A-8B), two pressure tubes were mounted normal to the fabric and were located just inside and outside of the sleeve. The pressure drop across the fabric was used to correlate local face velocities for varying ambient wind conditions on the fabric cylinder. Testing on an unconstrained sleeve, Figure A-8C, required gluing the 15.88 mm (0.625 in.) pressure tubes to the fabric. The pressure probes were located approximately 15.88 mm (0.625 in.) above the chordwise pressure ring. In order to acquire particle penetration data, a 3.175 mm (1/8 in.) diameter sampling probe was affixed to the inner core of the cylinder, see Figure A-9. This probe stood proud from the surface by approximately 6.35 mm (1/4 in.). An upstream sampling probe was located approximately 76 mm (3 in.) upstream and slightly below the downstream sampling probe for $\psi = 0$ deg. For non-zero azimuthal angles, the upstream probe was positioned as close as possible to the sleeve material, generally 13 mm (1/2 in.) upstream of the sleeve material.

BENCH TOP SWATCH TESTING

In order to determine the fabric face velocity variation with fabric pressure drop (and also to test basic fabric particle penetration characteristics), a bench top swatch testing apparatus was designed and built using a Pall Corporation 47 mm filter holder to test the fabric specimen. The results of the testing were utilized to correlate fabric face velocity and wind tunnel speed. The fabric face velocity was defined from reference 5 to be defined as:

$$U_O = \frac{Q}{A} \qquad \text{(cm/sec)} \tag{1}$$

where Q is the volumetric flow rate through the swatch and A is the cross-sectional area of the swatch exposed to the flow. Details of the bench top apparatus may be found in references 6 and 8.

PROCEDURE AND DATA REDUCTION

The NATF tunnel was allowed to thermally stabilize for over ½ hr before data acquisition commenced. Temperature was constant for a given tunnel speed, generally, 26.1ºC at 36.6 m/sec (79ºF at 120 ft/s). Isolated measurements of tunnel relative humidity were found to be 35%. After tunnel stabilization, pressure measurements were acquired for wind tunnel velocities of approximately 3 m/sec, 6 m/sec, 9 m/sec, 14 m/sec, 18 m/sec, 27 m/sec, and 36 m/sec. Repeat points were conducted at 3 m/sec and 36 m/sec. Post-test, the data were converted to pressure coefficient:

$$C_p = \frac{P - P_\infty}{q_\infty} \tag{2}$$

For particle penetration tests, sequential upstream/downstream particle samples were acquired after tunnel thermal stabilization. The sequential scans proceeded with the freestream sampling probe (upstream of the model) followed by the component sampling probe (internal to the sleeve). A total of 120 sec of data were taken for each scan for five downstream/upstream pairs. SMPS resolution was acquired at 64 channels per decade. For analysis the data was resolved to 16 channels per decade. Simultaneously, the APS acquired average concentration data over the SMPS sample period data. Particle penetration was determined by dividing the average downstream sample (in units of dN/d log Dp) by the average upstream sample (in units of dN/d log Dp, where N is the number of particles and Dp is the particle diameter size). The subsequent data was plotted as penetration[5] versus particle size (nm).

$$P = N_{down} \Big/ N_{up} \tag{3}$$

where N_{down} is the number concentration of particles downstream in a selected size channel and N_{up} is the number of particles upstream of diameter Dp.

Note: dN/d log Dp is the differential or normalized particle size distribution based on particle number and normalized to one decade of particle size. This normalized concentration format allows particle size distributions to be compared regardless of channel resolution. In this way the present data is comparable to data taken at other facilities and with other instrumentation.

Comparison of the initial upstream/downstream particle count measurement with the final upstream/downstream particle count measurements was used to determine if the test particles were loading the fabric. If the last upstream/downstream sequence was significantly different from the initial upstream/downstream sequence in particle count, this would be a sign of fabric loading and would lead to erroneous penetration values. No data reported in this paper was affected by detrimental fabric loading due to particle deposition.

It should be noted that numerous background particle measurements were acquired throughout the course of testing: these data were consistently below 10 counts per channel in the SMPS (and

in most cases much below this value) and negligible for measurements acquired by the APS at larger sizes. No long-term changes in these background levels were observed.

ERROR ANALYSIS AND DATA REPEATABILITY

As mentioned previously, the empty tunnel velocity spatial uniformity is approximately 1%. At a given spatial location in the test section, the tunnel velocity varied by approximately 0.5%. Tunnel temperature variations were less than 0.2°F in test. Experimental uncertainty was determined in a method outlined in reference 7 and the measured velocity was estimated to be with in ±1.45%. The pressure measurements, based on manufacturer's estimates, were accurate to ±0.05% full scale (after re-zero).

Because this method of testing sleeve components forms the basis for the development of a predictive tool to define penetration performance of a material, it was important to determine the robustness of the test set up and methodology. A number of repeat configuration tests and checks were conducted to assess the uncertainty of the entire system. This will be discussed in the next section.

RESULTS

RELATIONSHIP BETWEEN FABRIC FACE VELOCITY AND FABRIC PRESSURE DROP

A linear relationship between face velocity and fabric pressure drop was seen for various fabrics and is shown in Figure A-10. This is a common result for most fabrics, c.f., reference 5. Excepting the A30 material, increased slope of the curves was an indication of poor penetration performance. The permeability line on the figure is the average velocity of the flow of air passing through the material at a short distance ahead or aft of the textile sheet. In the United States, this velocity is determined at a pressure differential (ΔP) across the fabric face of 0.5 in. H_2O or 2.6 lb/ft2 (reference 10). The average permeability, standard deviation, and number of samples are provided in Table B-2. A separate, larger swatch fixture, developed for wind tunnel use, correlated with the bench top swatch testing. The data plotted in Figure A-10 was normalized to the average values of permeability for the fabrics shown in Table B-2. The number of samples for the averages ranged from 14 to 26.

PRESSURE VARIATION FOR THE COMPONENT (SLEEVE) MODEL

Following bench top swatch tests, component sleeve fixture testing was conducted in the NATF. Wind tunnel velocity was varied to determine the pressure variation on the model. Tests were conducted for the fixture: 1) without the support screen and without the fabric sleeve, 2) with the support screen but without the fabric sleeve, 3) with the support screen and with the fabric sleeve, and 4) without the support screen but with the fabric sleeve (limited testing).

Figure A-11 shows the pressure coefficient distribution for the case of the component sleeve fixture mounted in the wind tunnel without support screen and without fabric sleeve for the range of freestream velocities. The data were seen to match expected behavior for pressure coefficients about a circular cylinder for subcritical Reynolds numbers, reference 11. Due to alignment errors and wind tunnel cross flow error (typically much less than one deg), the stagnation location was seen to be slightly off from the assumed 0 deg azimuth location. Also plotted on the figure is an Akima curve fit (reference 12) of the 36 m/sec data. The curve fitted data had a maximum pressure coefficient of 0.98 which may be due to the limited angular resolution of the pressure data and alignment error/cross flow error.

With the addition of the support screen, see Figure A-12, a noticeable suction increase was seen to occur at the higher wind speeds similar to the flow around a circular cylinder above supercritical Reynolds numbers. Flow separation for the higher wind speeds was delayed from an azimuth angle of 75 deg to 120 deg. However, with the 10 oz. Denim fabric sleeve installed over the support screen, the pressure was found to nearly invariant with azimuth angle and ambient wind speed, see Figure A-13. The magnitude and trends shown in Figure A-13 were common for all materials tested. A similar behavior of constant pressure inside the gap between constrained fabric and inner cylinder was noted by Brasser (reference 13).

Removal of the support screen removed the gap between the sleeve and the inner cylinder on the windward side of the model. A stagnation-like pressure developed around an azimuth angle of 0

deg as ambient wind increased, see Figure A-14. At the lower speeds, the pressure coefficient was similar to the constrained sleeve suggesting the sleeve gaps were similar. It was noted during testing that there was significant flapping on the leeward side of the material. While it is possible to quantify the frequency of the unsteady motion, it is suspected that the motion is complex and dependent on a number of parameters (e.g., the mounting-induced tension of the material) that are not fully understood and require further study. Further, tension of the material is known to have an effect on fabric permeability (reference 14) and most likely penetration performance.

Figure A-15 compares the pressure difference between the leeward fabric pressure (point A on schematic in the figure) and the pressure on the inner cylinder at an azimuth angle of 0 deg (point B on the schematic in the figure). There is little difference in these pressures for the case of the constrained sleeve. However, for the case of the unconstrained sleeve, the pressure on the leeward fabric face, point A on the inset schematic, was noted to be significantly lower than the pressure measured on the inner cylinder at an azimuth angle of 0 deg, point B on the inset schematic. There was a variation on the pressure difference of the unconstrained data dependent upon fabric material. However, all unconstrained materials showed similar trends of an exponential increase in pressure differential.

Reference 15 developed a potential flow model for the case of a constant gap (constrained sleeve) to determine the pressure drop across the fabric:

$$\Delta P = \frac{4\rho V_\infty^2 \cos 2\Theta}{\beta^2 + 4} \tag{4}$$

where the coefficient β is calculated as:

$$\beta^2 = \frac{12\mu\alpha R^2}{\Delta R^2} \tag{5}$$

The pressure drop across the fabric at an azimuth angle of 0 deg is compared to potential theory in Figure A-16. The permeability for 10 oz. Denim was used for the potential flow model but surprisingly permeability was found to have little effect on the potential flow. As seen in the figure the fabric pressure drop is 30% lower than the potential flow model prediction at highest wind speed. Reference 5 noted improved correlation using a screen and material around the mounting fixture. However, the present test utilized a dummy mounting mechanism above the model to mimic the tunnel mounting hardware: it is doubted that asymmetrical differences in the flowfield account for the differences seen between the potential model and test data of Figure A-16. Regardless, spanwise pressure coefficients were noted to be invariant signifying notional two-dimensional flow.

A correlation between fabric face velocity and wind tunnel speed is shown in Figure A-17 and was determined knowing the pressure drop across the constrained sleeve at an azimuth angle of 0 deg and using the linear relationship between face velocity and pressure drop determined from bench top testing and shown in Figure A-10. The curves exhibit a non-linear increase in face

velocity with increasing wind speed. The relationship shown in Figure A-17 is used to correlate bench top penetration testing to component and wind tunnel swatch (reference 6) testing using a common parameter; face velocity.

Figures A-11 to A-14 show the pressure variation on the fixture inner core while Figure A-18 shows the azimuthal variation of the pressure differential across the fabric as a variation with model azimuth. For an azimuth of 0 deg, the data agree well with the data shown in Figure A-16. Note: The measurements of Figure A-16 were acquired in 2010 using a 20 in. of H_2O pressure module and the data seen in Figure A-18 were acquired in 2013 using a 10 in. of H_2O pressure module. Also shown in Figure A-18 are data from reference 16 on a similar sleeve fixture for an unidentified fabric. The maximum pressure differential values are provided in Table B-3. Overall, the reference data were seen to have similar pressure differential characteristics as the fabric tested in the present report but had a lower minimum pressure ratio that occurred at a larger azimuth angle. Possible explanations for this are: differences in solid blockage of the wind tunnel models in the flow, different materials, different methods to constrain the sleeve, and the absence of an inner core from reference 16. Reference 16 appears to have significant blockage in the testing duct. Blockage is generally defined as the ratio of model area to wind tunnel cross sectional area, reference 9. The present test had a blockage of 6.25%. Reference 16 does not provide dimensional details but images from the test suggest a blockage of approximately 50%. This very high blockage would lead to significant flow acceleration around the test specimen and would significantly affect the pressure measurements. Reference 16 had a better method to constrain the sleeve material compared to the screen used in the present report. The screen used in this report had slight asymmetries due to the method of fastening the ends together. This may lead to slight pressure differences as azimuth is varied. Reference 16 appears to not have an inner core in the test fixture. This would have a significant effect on the pressures inside the cylinder.

Using the a linear curve fit from Figure A-10, the data of Figure A-18 was converted to fabric face velocity as shown in Figure A-19. Only positive face velocities are plotted as this represents particle influx.

PARTICLE PENETRATION

CONTROL CHECKS

To gage the quality of the developed testing system, particle penetration tests were conducted on the component fixture devoid of a fabric sleeve but with the sleeve support screen (the configuration seen in Figure A-8a). As seen in Figure A-20, particle penetration was generally between 90% and 110% for $\psi = 0$ deg. Particle penetration data for $\psi = 15$ deg and $\psi = 30$ deg exhibited more scatter due to the difficulty in locating the upstream probe such that it was sampling the same flow as the downstream probe. The flow streamlines for non-zero yaw angles are not straight as the presence of the model causes the streamlines to diverge from the model/obstruction. To get the probe oriented such that both instruments performed adequately relative to the downstream generally took a day of trial-and-error testing. Of concern is the effect of the fabric sleeve on the flowfield. It is possible that the introduction of the fabric sleeve causes

the flowfield to change such that control check seen in Figure A-20 is no longer operative. Further study is warranted.

REPEATABILITY OF RESULTS

Figure A-21 shows typical repeatability for the sleeve test in the wind tunnel with DOS challenge using the SMPS and APS. Repeatability was found to be generally within 5% in particle penetration.

Typical downstream and upstream data are shown in Figure A-22a and b for a 10 oz Denim sleeve test using DOS as the challenge at a wind velocity of 18.3 m/sec and for $\psi = 0$ deg. The data was found to be repeatable and devoid of filter loading effects that would cause a variation in the downstream data over time for the tests.

For $\psi = 30$ deg and for a 10 oz Denim sleeve test using DOS as the challenge at a wind velocity of 18.3 m/sec the data was found to be repeatable and devoid of filter loading effects, see Figures A-23a and A-23b.

TIE-IN TO CLARKSON COMPONENT (SLEEVE) TESTS

Clarkson University personnel performed wind tunnel sleeve tests in 2007 using different instrumentation and software, mass flow controllers, and dissemination system, reference 5. As a check on the robustness of the developed techniques and systems, wind tunnel sleeve tests using the same challenge and material were conducted in 2013. As shown in Figure A-24, there is significant difference in the two measurements. Above 9.1 m/sec, the Clarkson data was found to have a lower maximum particle penetration compared to the NAVAIR data. The Clarkson test results had a maximum particle penetration greater than the NAVAIR data at 9.1 m/sec.

In addition, the Clarkson data exhibited a decrease in maximum particle penetration at 36.6 m/sec compared to the Clarkson data at 18.3 m/sec.

Reference 5 measured particle penetration using different flow rates through the downstream sample probe and found no change in particle concentrations downstream of the fabric, suggesting that the instrument sample flow rates were significantly smaller than the ambient wind-driven flow flux. Therefore, any differences between NAVAIR and Clarkson instrumentation flow rates are unlikely to explain the differences seen in Figure A-24. However, the effect of the downstream sampling probe azimuthal location was found to have an effect on downstream particle concentration, suggesting the air volume between the outer fabric cylinder and the inner cylinder is not well mixed. The tests of reference 5 chose a downstream sampling probe located between $\Theta_{probe} = \sim 30 - 60$ deg based on the location that yielded the maximum particle penetration value. The NAVAIR sampling probe was located at $\Theta_{probe} = 0$ deg for $\psi = 0$ deg (and $\Theta_{probe} = \psi$ for non-zero yaw angles). This may explain the differences seen in Figure A-24.

EFFECT OF INCREASING WIND VELOCITY ON PENETRATION AT CONSTANT YAW ANGLE

Particle penetration measurements were determined for yaw angles of 0, 15, and 30 deg. As seen in Figure A-18, yaw angles above 30 deg have an outflow of particles. Figure A-25 shows the effect of increasing wind velocity at $\psi = 0$ deg yaw angle on particle penetration through a 10 oz Denim sleeve test using a DOS challenge. For sub-micron sizes where the peak particle penetration occurred, a general trend of increasing wind speed exhibited increased penetration. High sub-micron to micron-sized particles tended to increase in particle penetration with wind velocity until 9 m/sec. Higher wind speeds tended to a see a reduction in particle penetration. This phenomenon is explained by single fiber filter efficiency models, references 5 and 7.

As shown in Figures A-26 and 27, show the effect of the various filter mechanisms (i.e., impaction, interception, and diffusion) has on the total filter efficiency for a low and a high fabric face velocity. Impaction occurs when a particle is unable to follow a streamline around a fiber because of inertial effects and impacts the fiber. Interception occurs when a particle follows its streamline but that streamline is within one particle radius of a fiber. The particle hits the fiber and is captured. Diffusion transport occurs because of the effect of Brownian motion. Brownian motion is the irregular motion of a particle in still air caused by random variation of gas molecules against the particle, reference 7. The random motion greatly increases the probability of a particle striking a fiber and being capture. Very small particles not subjected to high face velocities are captured mainly by diffusion, see Figure A-26. As particle size increases, interception becomes the primary filtration mechanism (with impaction being slightly lesser in importance). As face velocity is increased, see Figure A-27, interception and impaction cause an increase in overall filter efficiency. Nearly all large particles are captured with the primary filtration mechanism being impaction.

Increasing the yaw angle to $\psi = 15$ deg is seen to result in lower overall particle penetration for a given wind speed compared to the $\psi = 0$ deg case (Figure 28). As yaw angle is further increased to $\psi = 30$ deg, the effect of wind speed on the particle penetration is greatly diminished to the point that particle penetration differences are slightly greater than the uncertainty of the experiment, see Figure A-29.

EFFECT OF INCREASING YAW ANGLE ON PENETRATION AT CONSTANT WIND VELOCITY

Figures A-30 through A-34 shows the effects of increasing yaw angle on fabric penetration for a given wind speed using a DOS challenge. In general as yaw angle is increased, particle penetration decreases. This follows the general trend shown in Figures A-18 and A-19: as yaw angle is increased, the fabric pressure drop and computed face velocity decrease.

At the lowest wind speed of 9.1 m/sec in Figure A-30, there was little difference in particle penetration for the non-zero yaw angles. It was hoped that differences in fabric face velocity at a given yaw angle could be used to easily predict particle penetration. Unfortunately, the mechanism is not quite that simple. Figure A-19 shows little difference in computed face

velocity at a wind speed for all the yaw angles tested at a wind velocity of 9.1 m/sec. While the non-zero yaw angles exhibit the same particle penetration characteristics, $\psi = 0$ deg particle penetration data is significantly greater.

As wind velocity is increased, maximum particle penetration decreases with increasing yaw angle, see Figures A-31 to A-33. However, large sub-micron to micron sized particles tend to collapse to the same penetration value as wind tunnel velocity is increased, irrespective of yaw angle.

DISCUSSION

It was hoped that particle penetration data would exhibit a direct correlation with fabric pressure drop/fabric face velocity and bench top testing could be used to predict particle penetration performance at equivalent wind velocities for non-zero yaw angles. The present technique shows promise to predict particle performance: the general trend of a decrease in fabric pressure drop/fabric face velocity results in a decrease in particle penetration through the fabric. However, fabric pressure difference/fabric face velocity is not the sole parameter to identify particle penetration. There may be an aerodynamic/particle dynamic aspect that is not being taken into account.

Figures A-34 and A-35 compare material penetration performance grouped loosely by face velocity. As seen in Figure A-34, face velocities between 2.8 cm/sec and 3.7 cm/sec exhibited similar penetration performance excepting the 9.1 m/sec at $\psi = 0$ deg data set which was much higher. For a range of face velocities between 6 cm/sec to 10 cm/sec shown in Figure A-35, the use of face velocity solely as a predictive tool for penetration performance breaks down.

Differences between the pressure on the leeward side of the fabric (point A in the schematic in the Figure) and the corresponding pressure tap on the model inner core as a variation of azimuth (point A in the schematic in the figure) are plotted and shown in Figure A-36. Pressure differences were found to be negligible and exhibited similar trends as the pressure on the inner core with a constrained fabric (e.g., Figure A-13). A significant difference between the two pressures would indicate internal flow and the location of the downstream probe relative to the fabric may be important. The negligible pressure difference does not explain the penetration differences between $\psi = 0$ deg and $\psi = 15$ deg data seen in Figures A-34 and A-35.

The differences between the pressure on the leeward side of the fabric and the corresponding pressure tap on the model inner core seen for the unconstrained sleeve in Figure A-15 (points A and B in the inset schematic) are difficult to understand and explain. It was thought that the unconstrained fabric would lie on the inner core at an azimuth of $\psi = 0$ deg and images suggest that occurred under wind load. Under such circumstances, pressure differences would be assumed negligible. The decided difference in pressure between the leeward side of the fabric (point A) and the corresponding pressure tap on the model inner core (point B) suggests that the unconstrained sleeve penetration performance may be difficult to repeatedly obtain. However, it is possible the finite pressure tubing (approximately 2.3 mm) caused a gap with significant flow and explains the pressure difference. The test should be repeated but with the leeward probe moved vertically upward and inch or two to not influence the inner core pressure tap.

As was mentioned, it was very difficult orienting the upstream probe for non-zero yaw angles so that the upstream and downstream probes measured the same number of particles and size distribution without a sleeve on the model. No one location resulted in both instruments measuring 100% particle penetration between the upstream and downstream sampling probes. This necessitated a compromised orientation so that the two instruments measured particle penetration as close as practicable to 100%. Even with these difficulties and taking into account the resulting increased uncertainty of the non-zero yaw angle data, the resultant trends are still

measurable and consistent: i.e., increasing yaw angle leads to a decrease in particle penetration through the fabric.

However, what is not known, and difficult to quantify, is the effect of the sleeve on the particle streamlines, and thus the penetration performance. It is suspected that this effect becomes a concern when fabric permeability is decreased. For the present test, it is estimated that the uncertainty could be as high as ±10% for particle penetration based on the range of penetration found during probe orientation runs. Further research could determine the effect of the sleeve on the flow using Particle Image Velocimetry (PIV).

CONCLUSIONS

Tests were conducted to determine the azimuthal pressure characteristics of a circular cylinder with a simulated fabric sleeve. A support screen was placed between the fabric and the circular cylinder to create an idealized flow condition with a constant air gap. With the constrained sleeve, the pressure coefficient around the model inner core was measured and found to be nearly invariant with azimuth and wind velocity and had a value of approximately -0.5. Fabric pressure drop was measured as a variation with model azimuth and found to exhibit a net inflow for azimuth angles less than 30 deg. Larger azimuths exhibited positive pressure differences indicating a net outflow through the material.

A methodology was developed to test component (sleeve) specimens at elevated wind speeds in the NATF wind tunnel. The developed dissemination system was found to be temporally and spatially repeatable. Particle penetration was measured for three yaw angles and at four wind speeds. In general the maximum particle penetration was found to increase with increasing wind velocity and decrease with increasing yaw angle. The results were found to be consistent and repeatable.

Fabric pressure differential/fabric face velocity was to be a parameter, but not the sole parameter, to quantify particle penetration performance. Further research or analysis may be needed quantify this complex phenomenon completely.

RECOMMENDATIONS

The results from this test are part of an initial development of a component, or simulated sleeve, testing methodology. However, this work is still in its infancy and much work needs to be accomplished to understand the flow physics inside and outside the component, the dynamics of material flapping, the effect of closures and seams, and particle penetration and deposition.

Computational modeling should be developed in parallel with the experimental effort to aid in the design of new fielded systems. Full-system tests should be carried out to determine if the modeling and experimental predictions and the testing methodology developed are adequate.

Penetration tests with unconstrained sleeves should be conducted.

New particles with discreet properties, such as size and fluorescent excitation frequency uniqueness will need to be developed to assist in deposition measurements. The overall goal should be both an improved testing methodology and improved design capability.

REFERENCES

1. Performance of Protective Clothing: Issues and Priorities for the 21st Century edited by Henry, N.W., and Nelson, C.N. ASTM Special Technical Publication//Stp, ASTM International. Jul 2000.

2. Bouskill, L.M., Kuklane, K., Holmer, I., Parsons, K.C., Withey, W.R., "The Relationship Between Ventilation Index and Thermal Insulation." *Proceedings of the 8th International Conference on Environmental Ergonomics*, San Diego, CA, Oct 1998.

3. Irshad, H., McFarland, A.R., Landis, M.S., Stevens, R.K., "Wind Tunnel Evaluation of an Aircraft-Borne Sampling System," *Aerosol Science and Technology*, 38:311-324, 2004.

4. Stewart, V.R., "Naval Air Warfare Center, Warminster, PA Aerodynamic Test Facility Operation Instructions," KSA Technology Report, Columbus, OH, Aug 1996.

5. Hill, M.A., Dhaniyala, S., Ghee, T.A., Kaufman, J., "Investigation of Aerosol Penetration through Individual Protective Equipment in Elevated Wind Conditions." Presented at the AAAR 26th Annual Conference, Reno, NV, September 2007. NAWCADPAX/TR-2012/365, 1 Mar 2013. Aerosol Science and Technology, Volume 47, Issue 7, pp. 705-713, Apr 2013.

6. NAWCAD Patuxent River Technical Report No. NAWCADPAX/TR-2014/7, Swatch Testing at Elevated Wind Speeds, of Jul 2014.

7. Hinds, W.C., Aerosol Technology, Second Edition, John Wiley & Sons, Inc., New York, New York, 1999.

8. Ghee, T.A., Murphy, K.L., "A Method to Correlate Ambient Wind to Fabric Face Velocity and Permeability." AIAA-2011-311. Proceedings of the 49th AIAA Aerospace Sciences Meeting, Orlando, FL, Jan 2011.

9. Barlow, J., B., Rae, W.H., Pope, A. Low-Speed Wind Tunnel Testing, 3rd Edition, Wiley, New York, 1999.

10. Hoerner, S.F., Fluid-Dynamic Drag, Hoerner Fluid Dynamics, Vancouver, Washington, 1965.

11. Schlichting, H., Boundary Layer Theory, 7th ed., McGraw-Hill, New York, NY, 1979.

12. Akima, H., "A New Method of Interpolation and Smooth Curve Fitting Based on Local Procedures", Journal of the Association for Computing Machinery. Vol. 17, No. 4, Oct 1970.

13. Brasser, P., "Theoretical and Experimental Study of Airflow Through Clothing Around Body Parts," American Institute of Chemical Engineers Journal Vol. 52, No. 11, Nov 2006.

14. Payne, P.R., "The Theory of Fabric Porosity as Applied to Parachutes in Incompressible Flow," *The Aeronautical Quarterly*, Vol. 29, No. 3, 1978.

15. Bergman, W., Fedele, P.D., McCallen, R., Sutton, S., "Hydrodynamically Induced Aerosol Transport," *Proceedings of the 1985 Scientific Conference on Chemical Defense Research*, Aberdeen Proving Ground, MD, Apr 1986.

16. Bergman, W., Garr, J., Fearon, D., "Aerosol Penetration Measuremnts Through Protective Clothing in Small Scale Simulation Tests." *Proceeding of the Third International Symposium on Protection Against Chemical Warfare Agents*, Umeå, Sweden, Jun 1989.

APPENDIX A
FIGURES

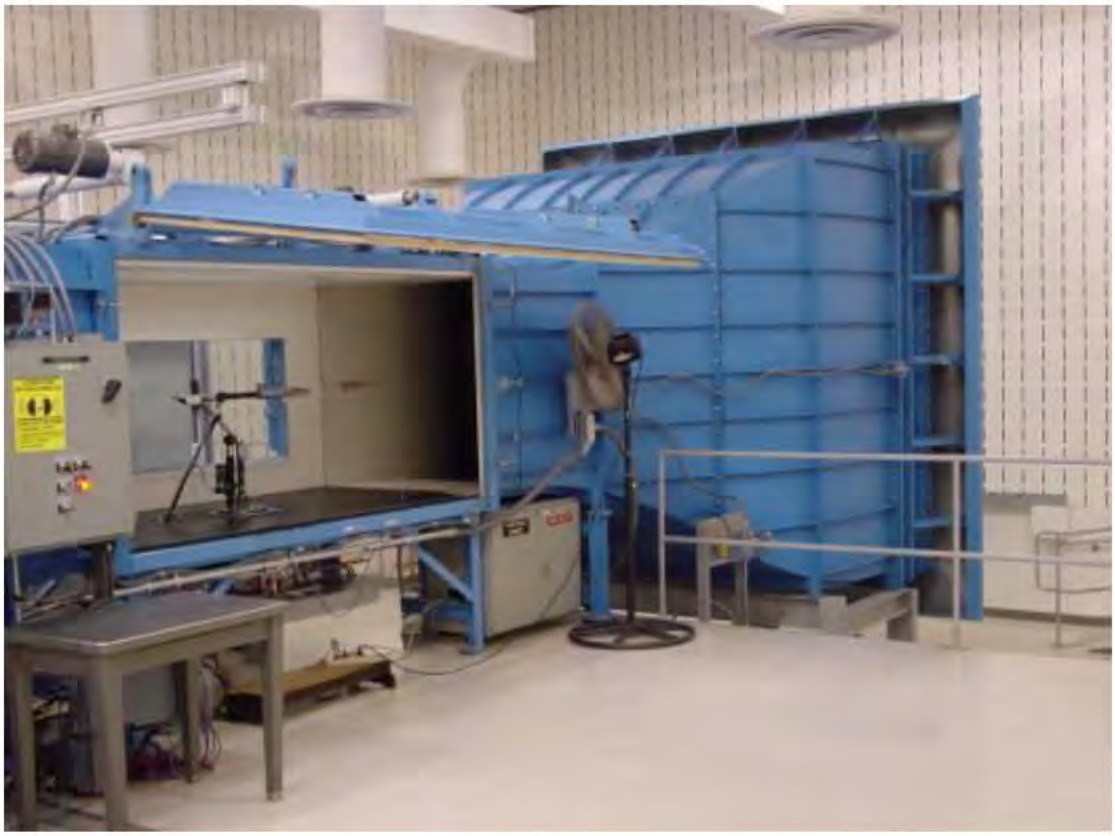

Figure A-1: NATF

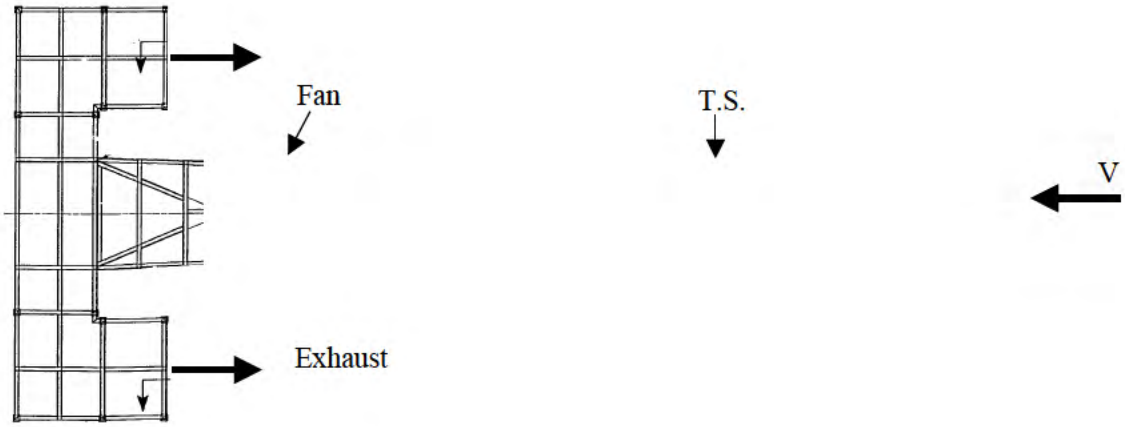

Figure A-2: Schematic of NATF

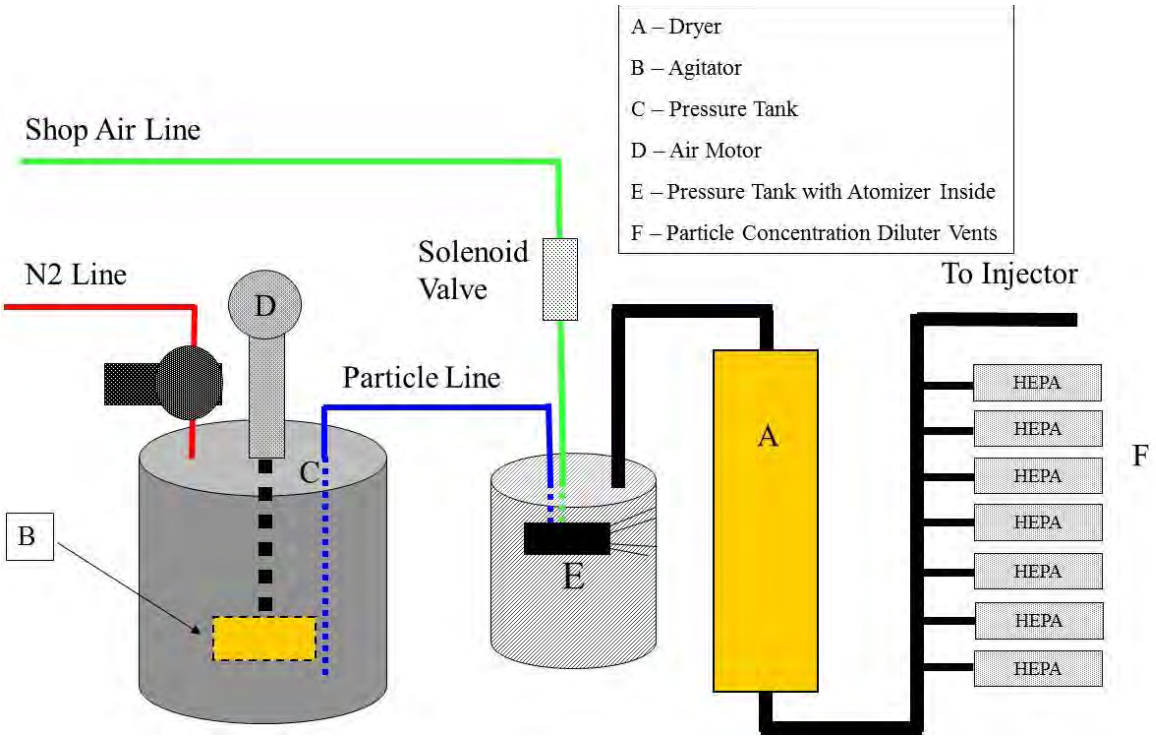

Figure A-3: Schematic of DOS Dissemination System

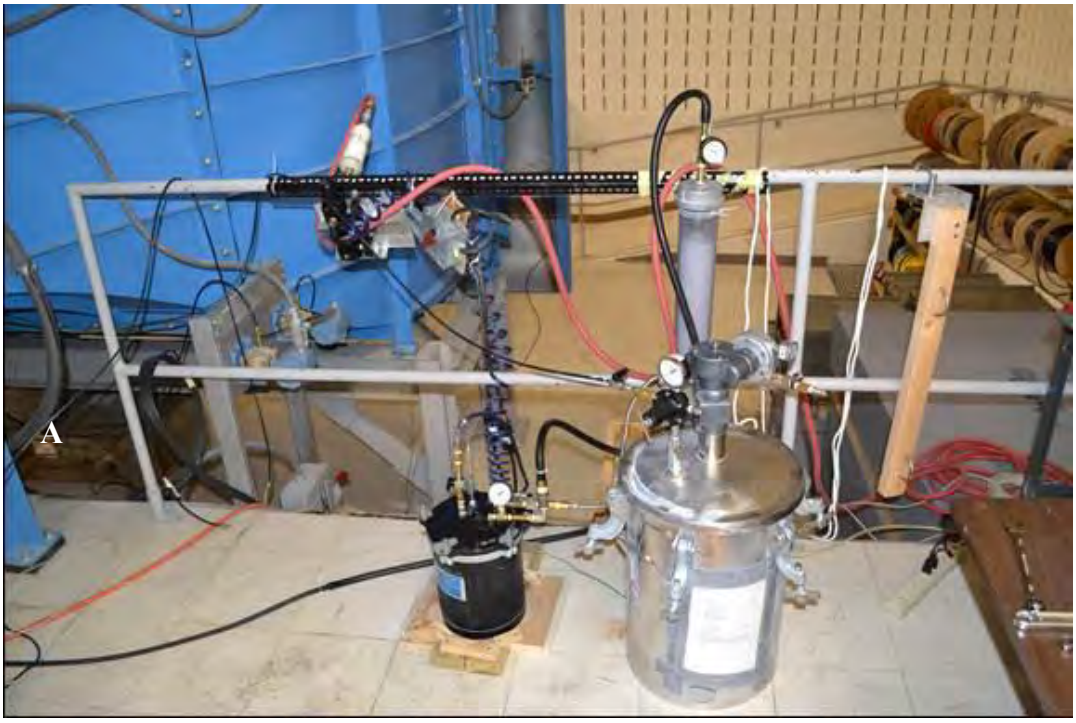

Figure A-4: DOS Dissemination System

Figure A-5: Wind Tunnel Ejectors, Inset: Front View

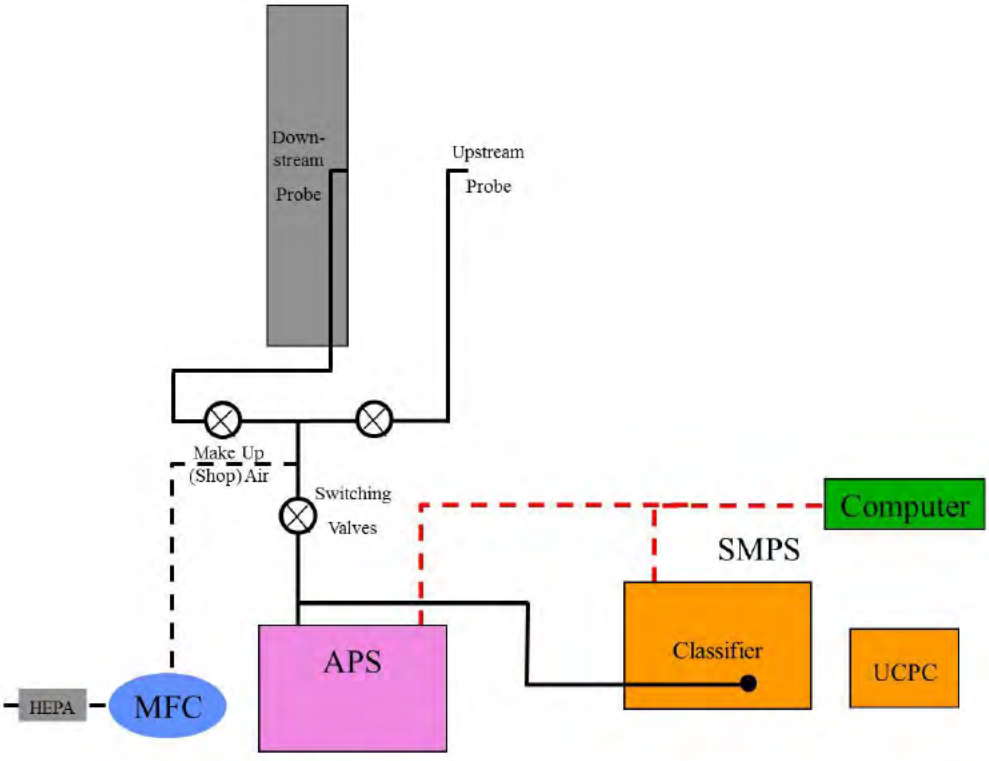

Figure A-6: Schematic of Wind Tunnel Sleeve Fixture Sampling DOS Challenge

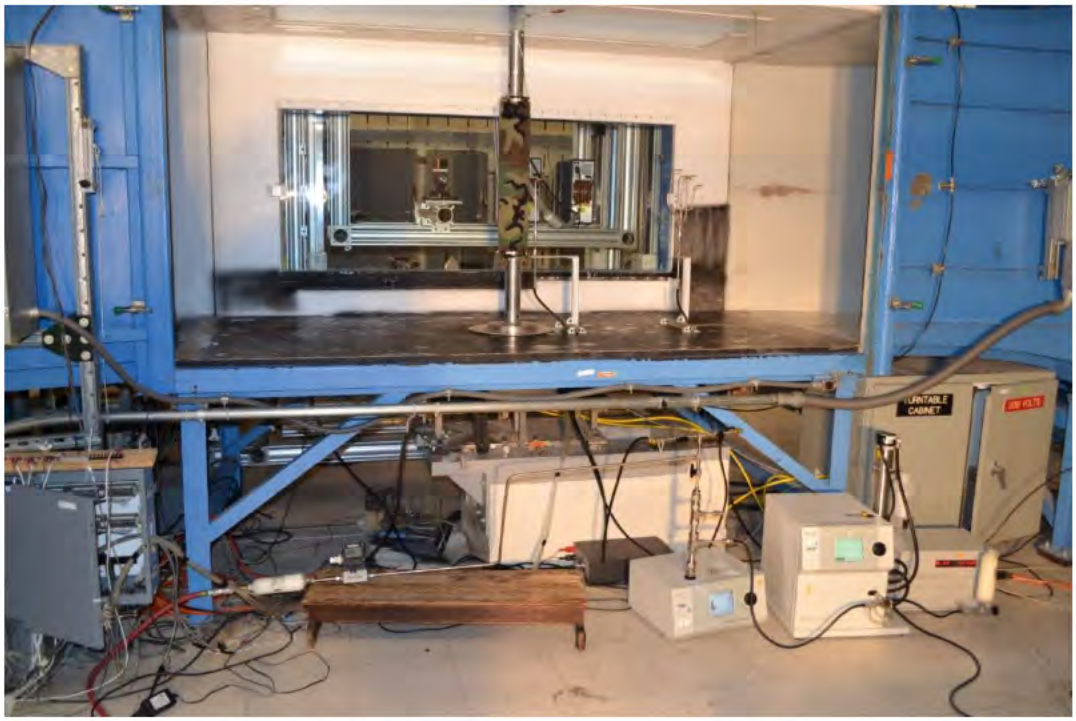

Figure A-7: Test Set-Up for Wind Tunnel Sleeve Testing

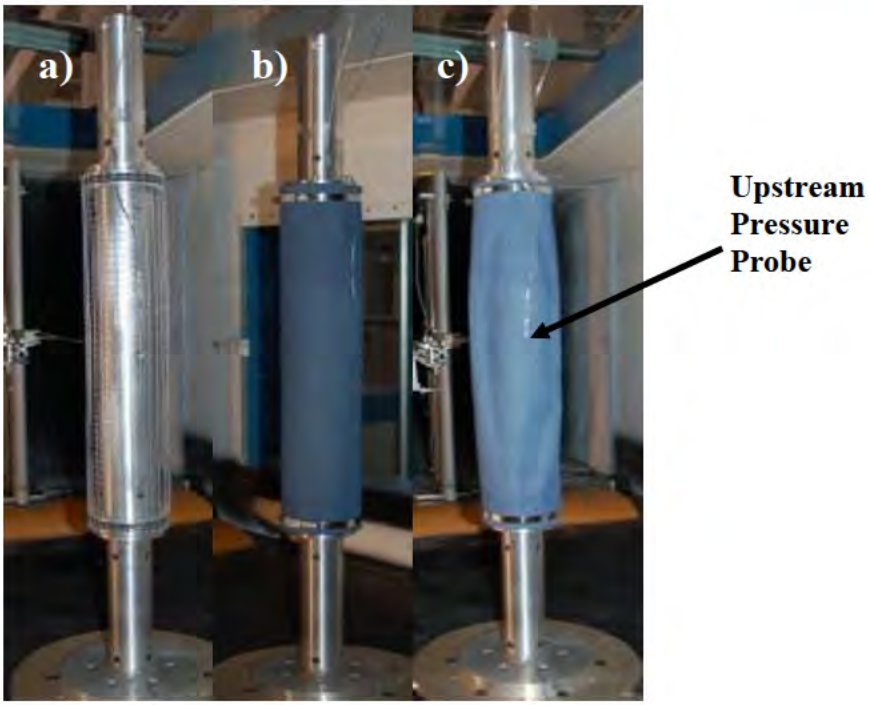

Figure A-8: Component Fixture a) Support Screen, b) with Installed Sleeve over Support Screen, c) with Installed Sleeve w/o Support Screen

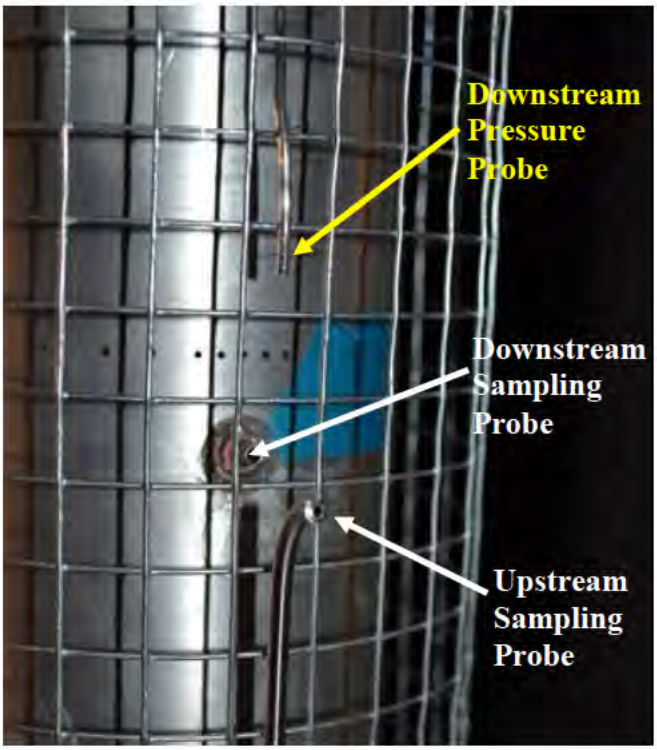

Figure A-9: Front of Wind Tunnel Swatch Holder with Upstream Sampling Probe and Static Pressure Probe

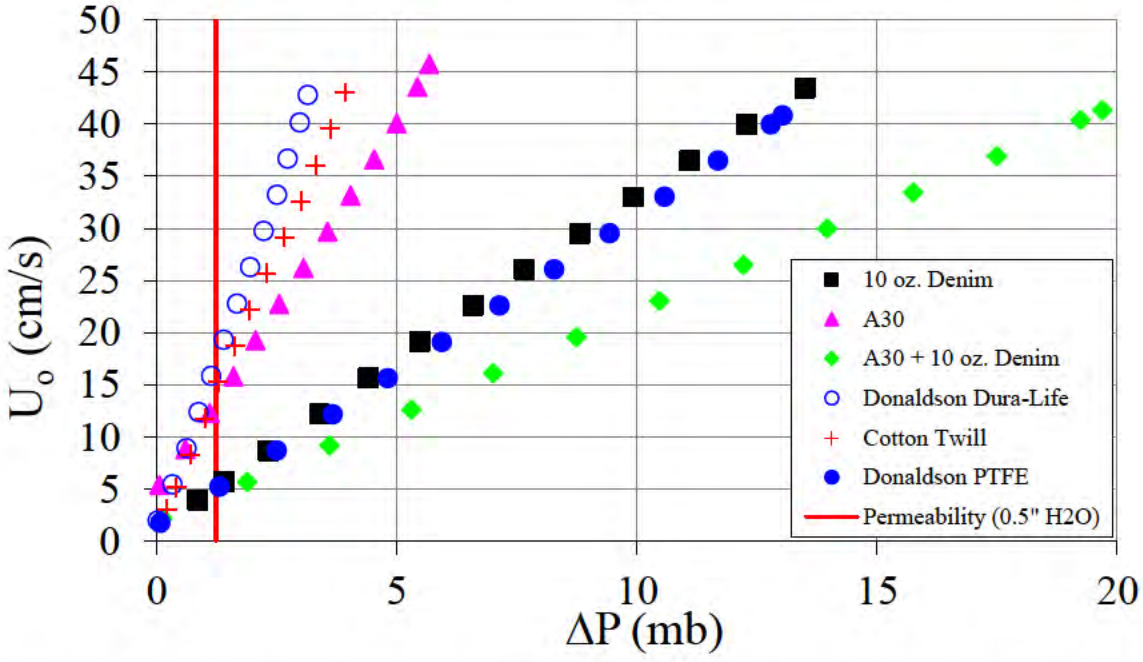

Figure A-10: Face Velocity Variation with Pressure Drop for Various Materials (Bench Top)

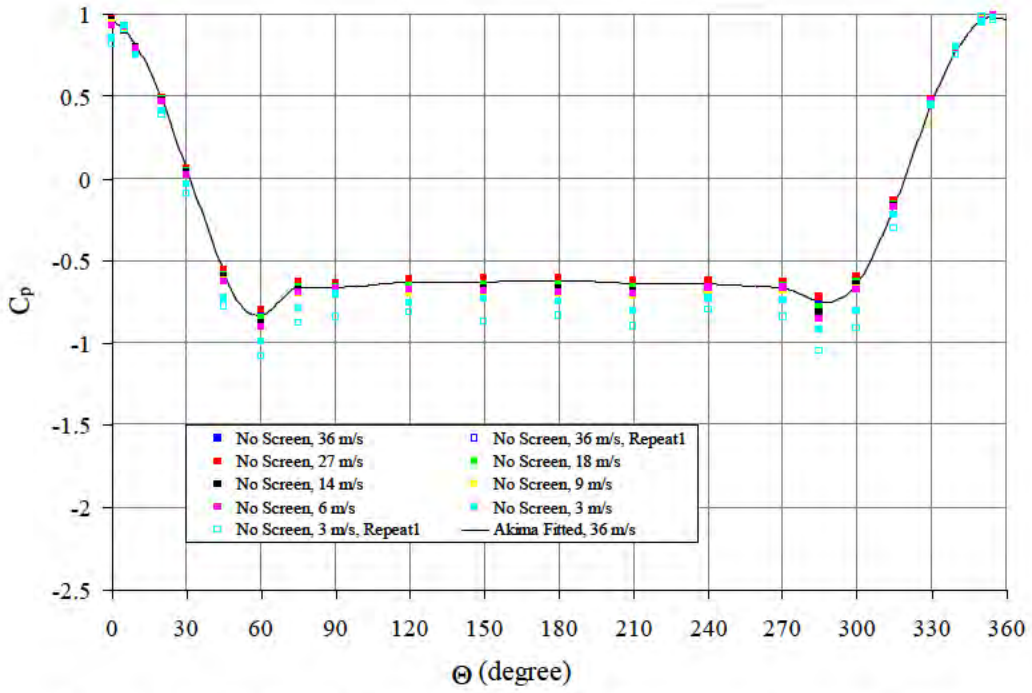

Figure A-11: Pressure Distribution Around Component Sleeve Fixture (w/o Sleeve, without Screen)

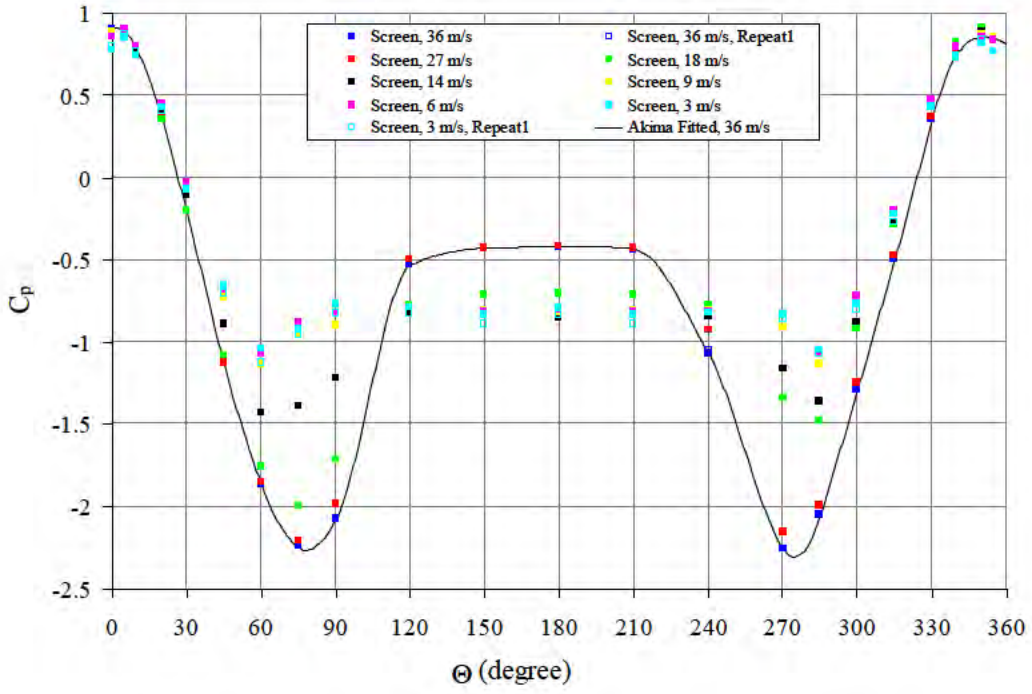

Figure A-12: Pressure Distribution Around Component Sleeve Fixture (w/o Sleeve, with Screen)

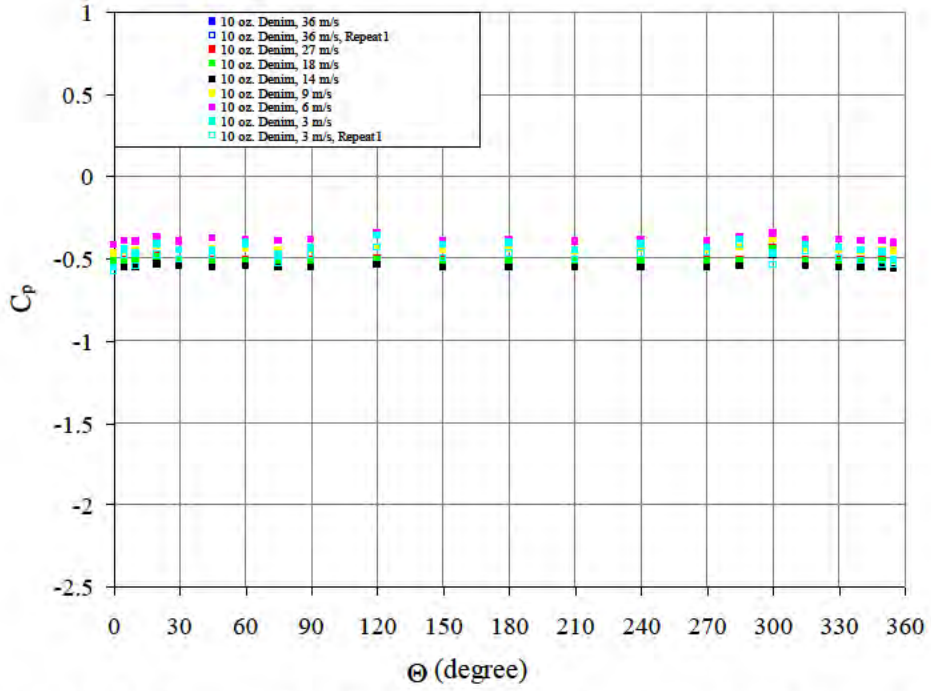

Figure A-13: Pressure Distribution Around Component Sleeve Fixture, with 10 oz. Denim Sleeve, with Screen

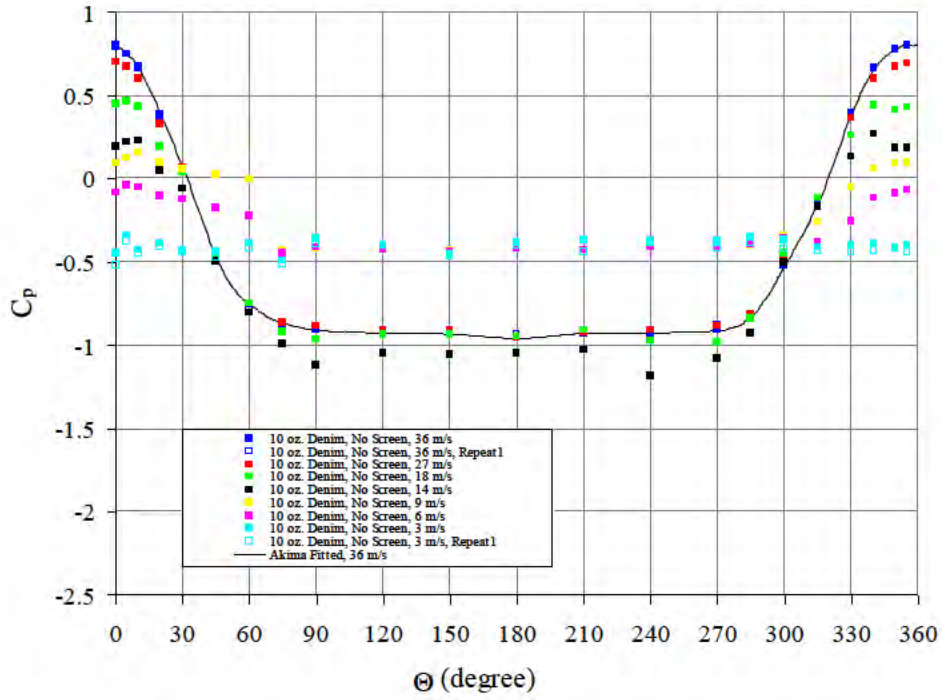

Figure A-14: Pressure Distribution Around Component Sleeve Fixture, with 10 oz. Denim Sleeve, w/o Screen

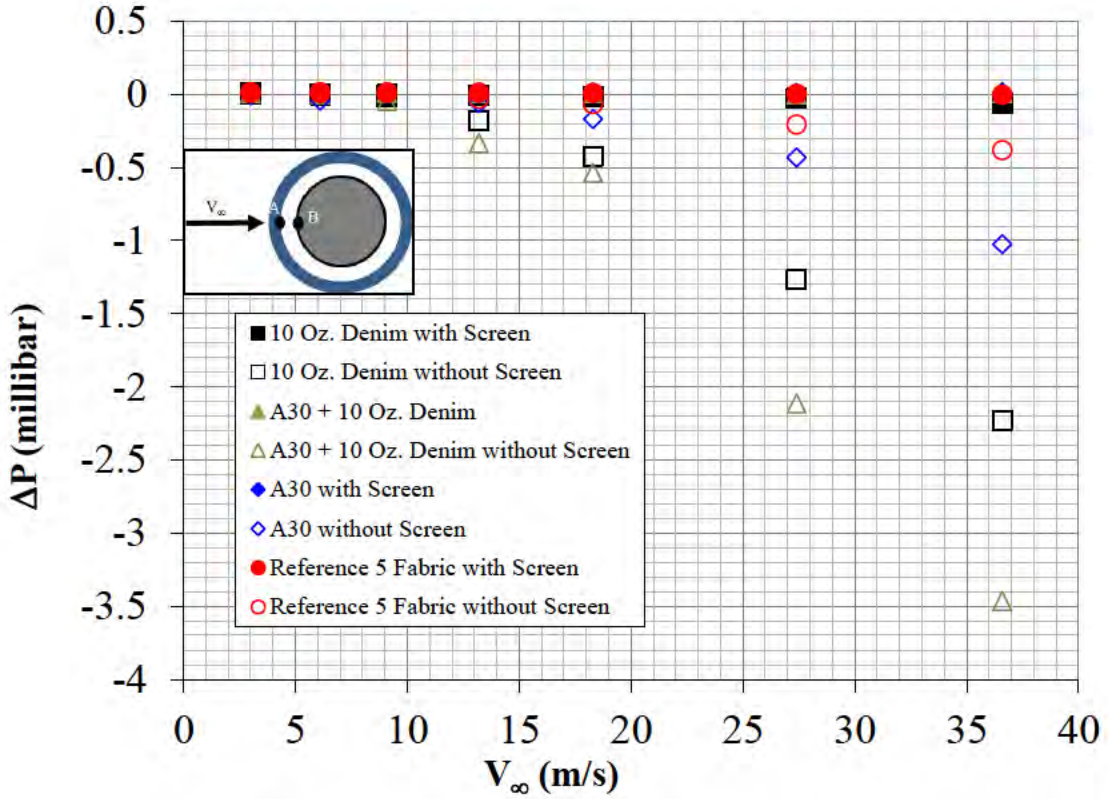

Figure A-15: Pressure Difference between Leeward Fabric Pressure and Inner Cylinder Pressure Tap at 0 deg Azimuth for Various Materials

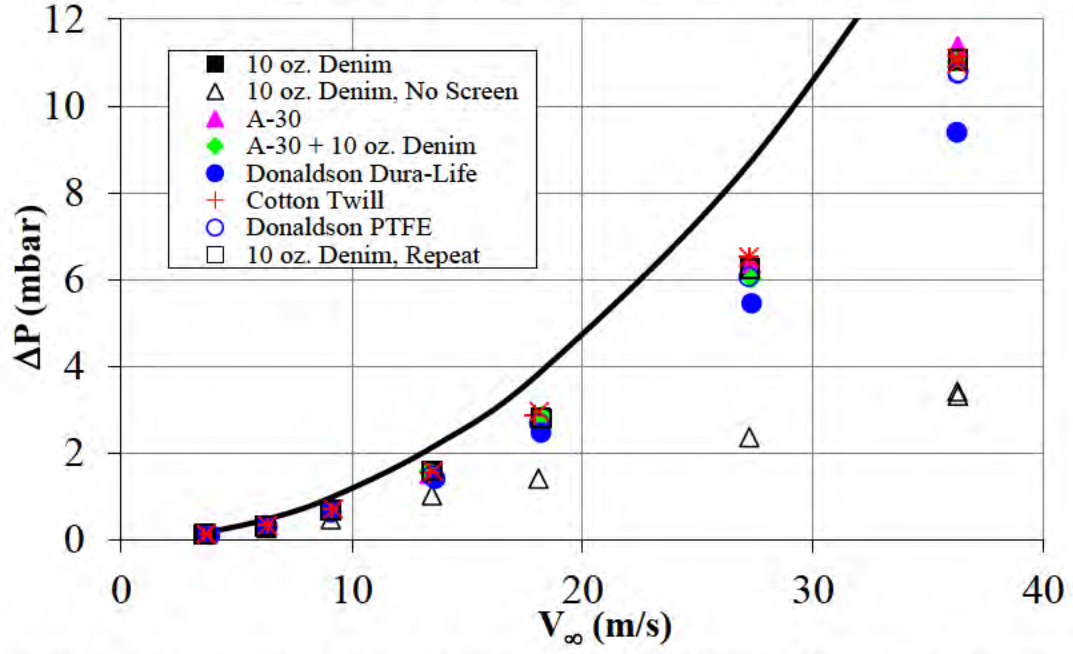

Figure A-16: Fabric Pressure Drop as a Variation with Wind Tunnel Velocity at Stagnation Point for a Variety of Fabrics

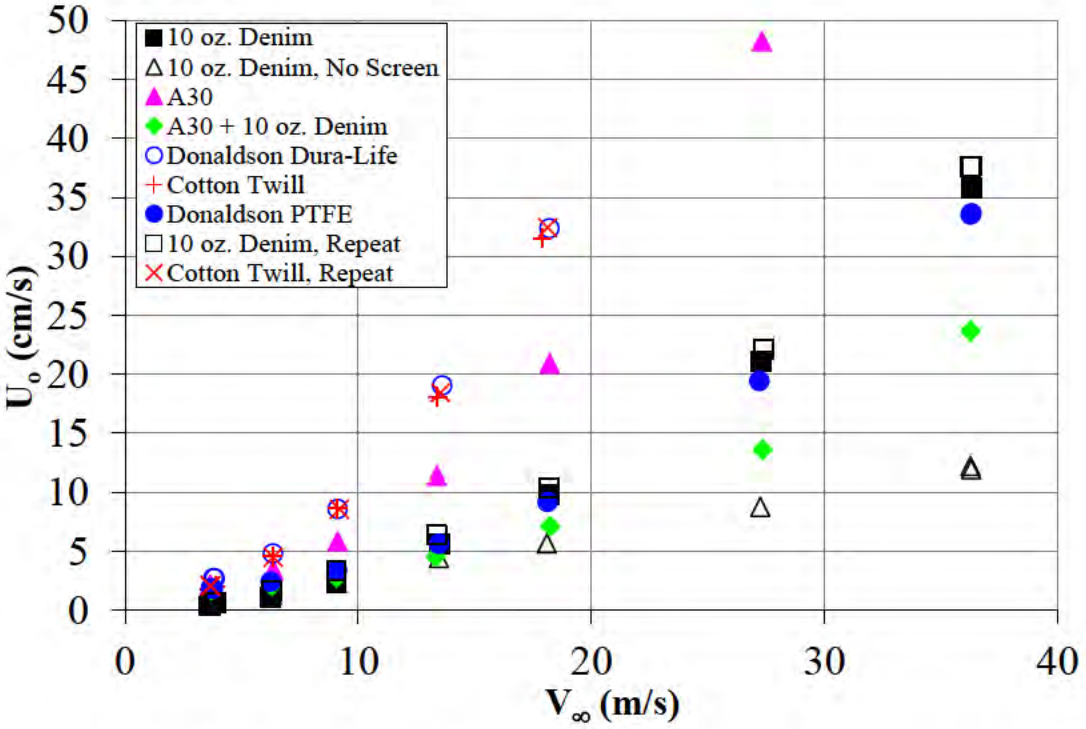

Figure A-17: Face Velocity Variation with Wind Tunnel Speed Determined from Wind Tunnel Sleeve Testing

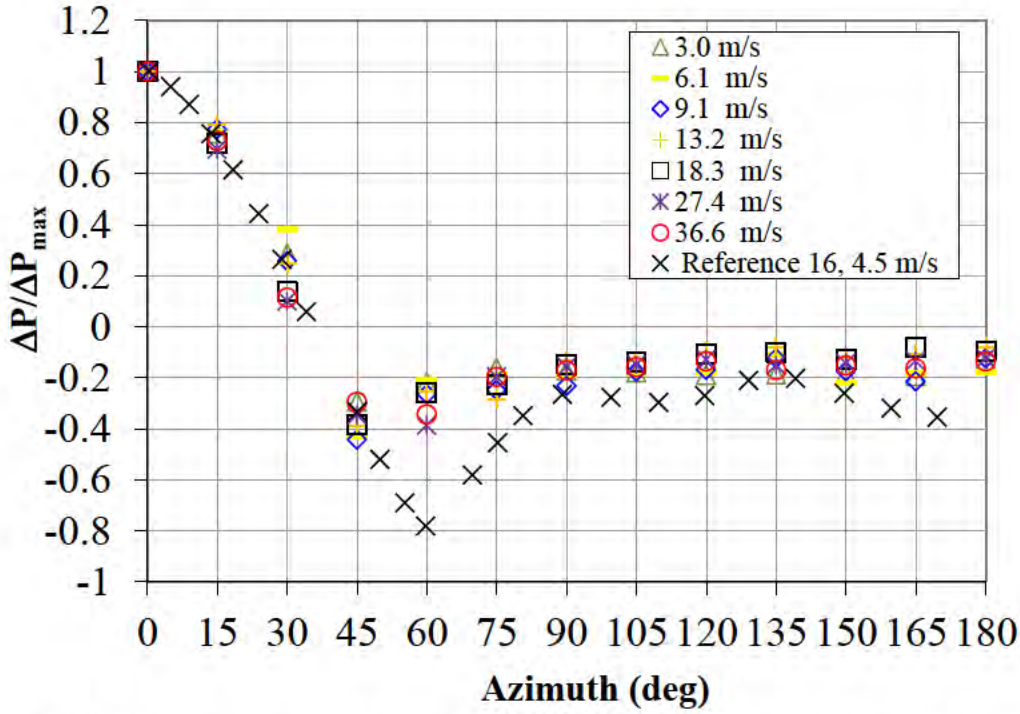

Figure A-18: Fabric Pressure Differential Variation Around Azimuth, 10 oz. Denim with Screen

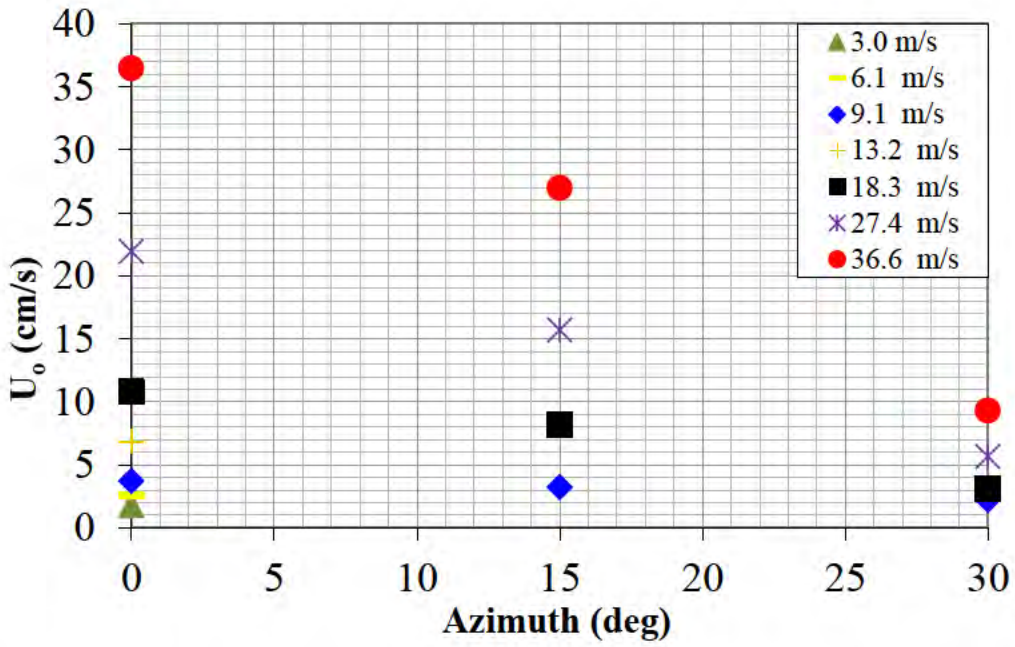

Figure A-19: Face Velocity Variation with Azimuth, 10 oz. Denim with Screen

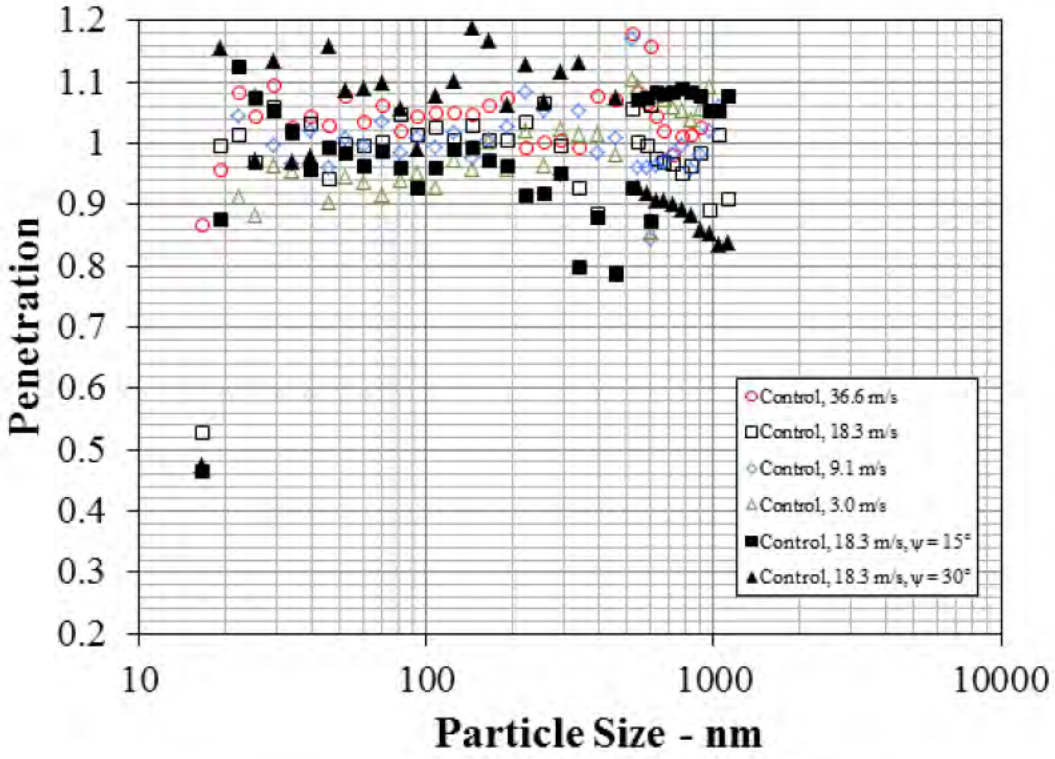

Figure A-20: Control Penetration (No Sleeve) Check

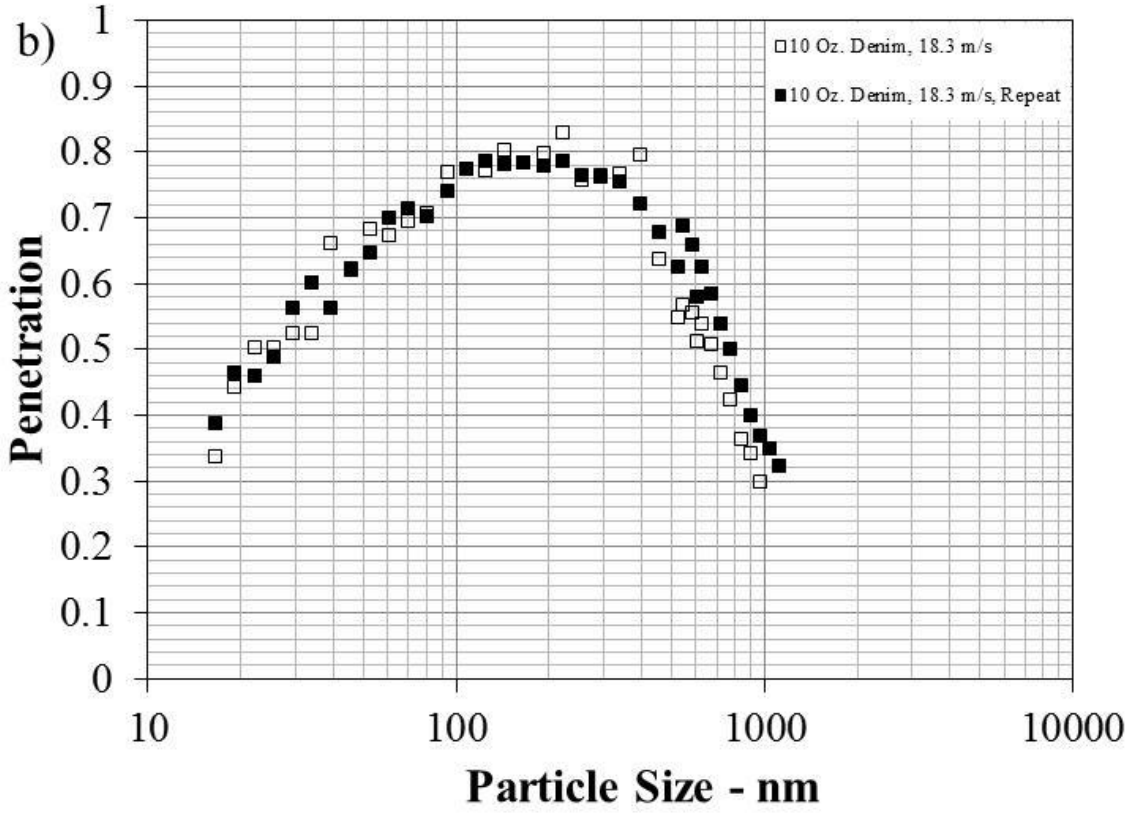

Figure A-21: System Repeatability, Wind Tunnel Sleeve Testing, 18.3 m/sec

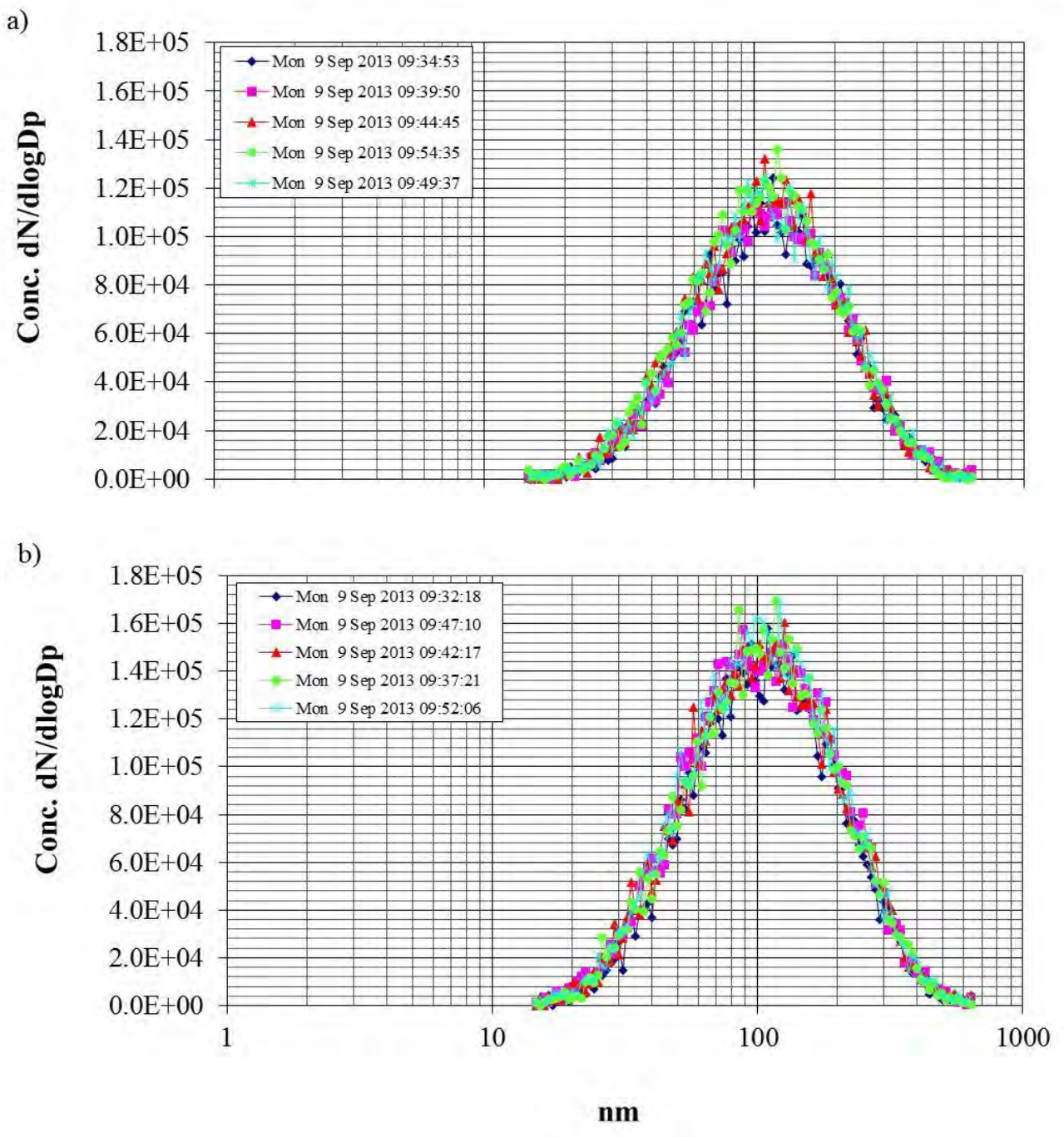

Figure A-22: Typical in-Test Repeatability, 10 oz. Denim, 18.3 m/sec, $\psi = 0$ deg:
a) Downstream Sample, b) Upstream Sample

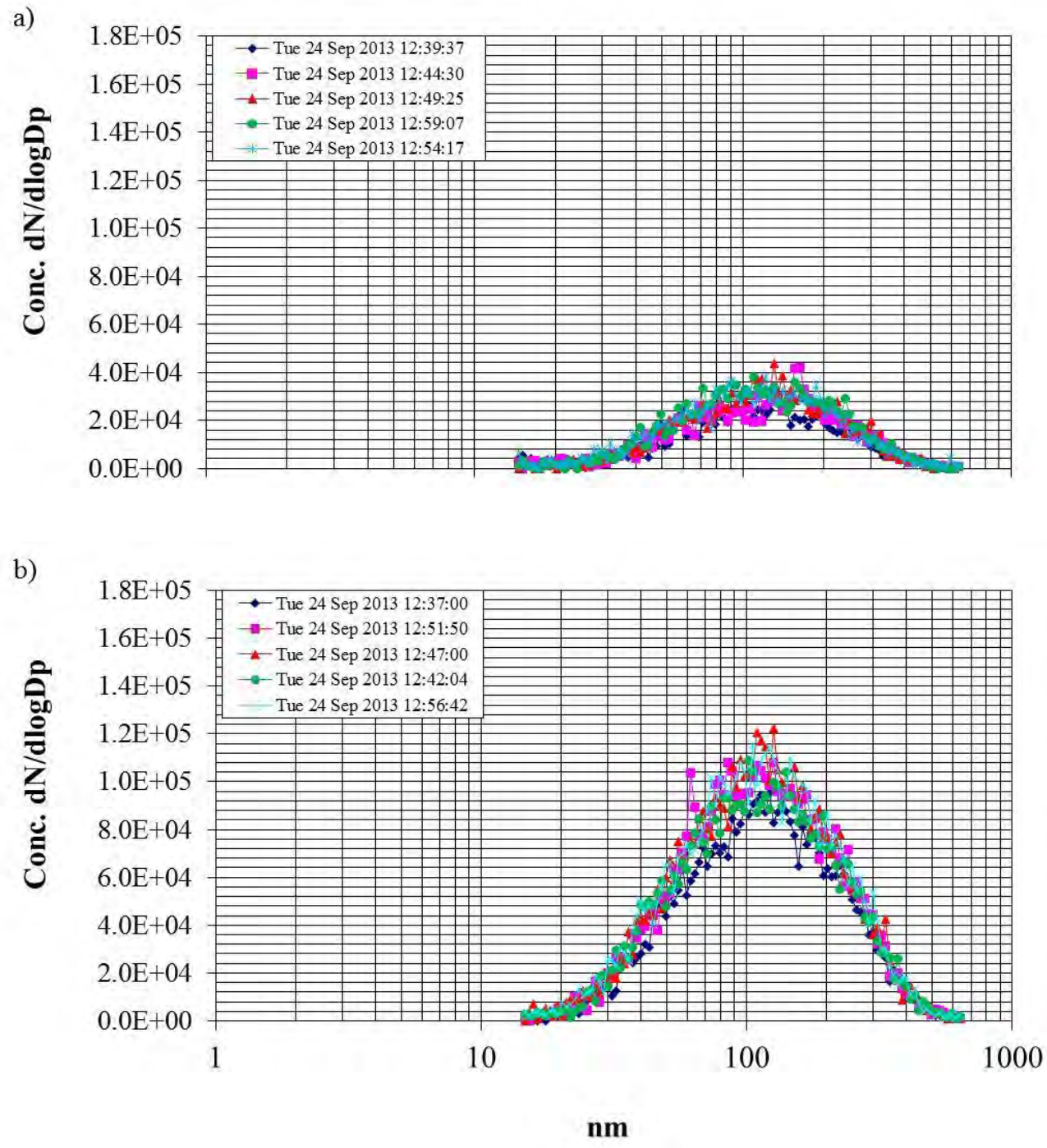

Figure A-23: Typical in-Test Repeatability, 10 oz. Denim, 18.3 m/sec, ψ = 30 deg:
a) Downstream Sample, b) Upstream Sample

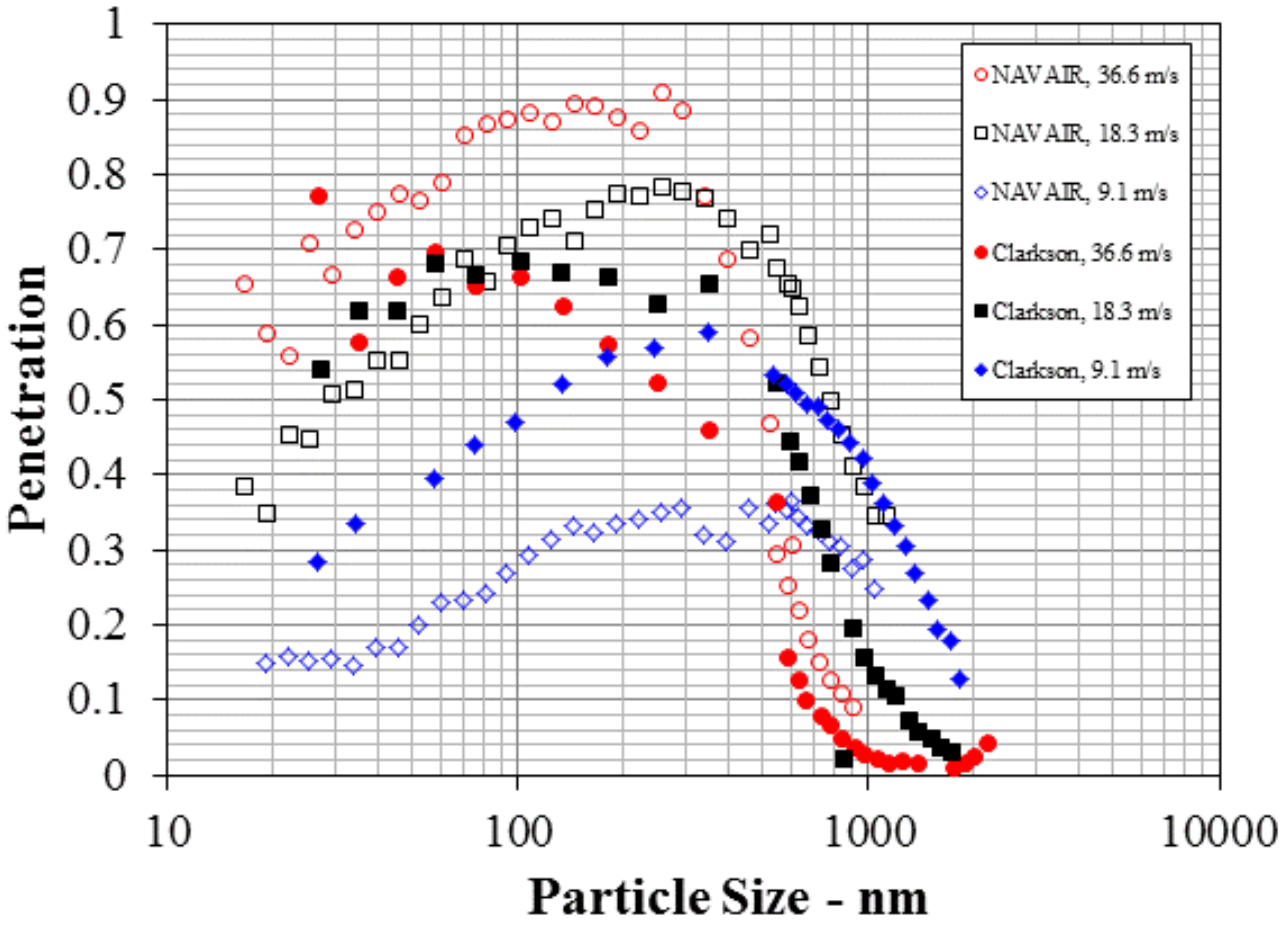

Figure A-24: Comparison of Clarkson and NAVAIR Wind Tunnel Sleeve Test Systems
(Clarkson Data from reference 5)

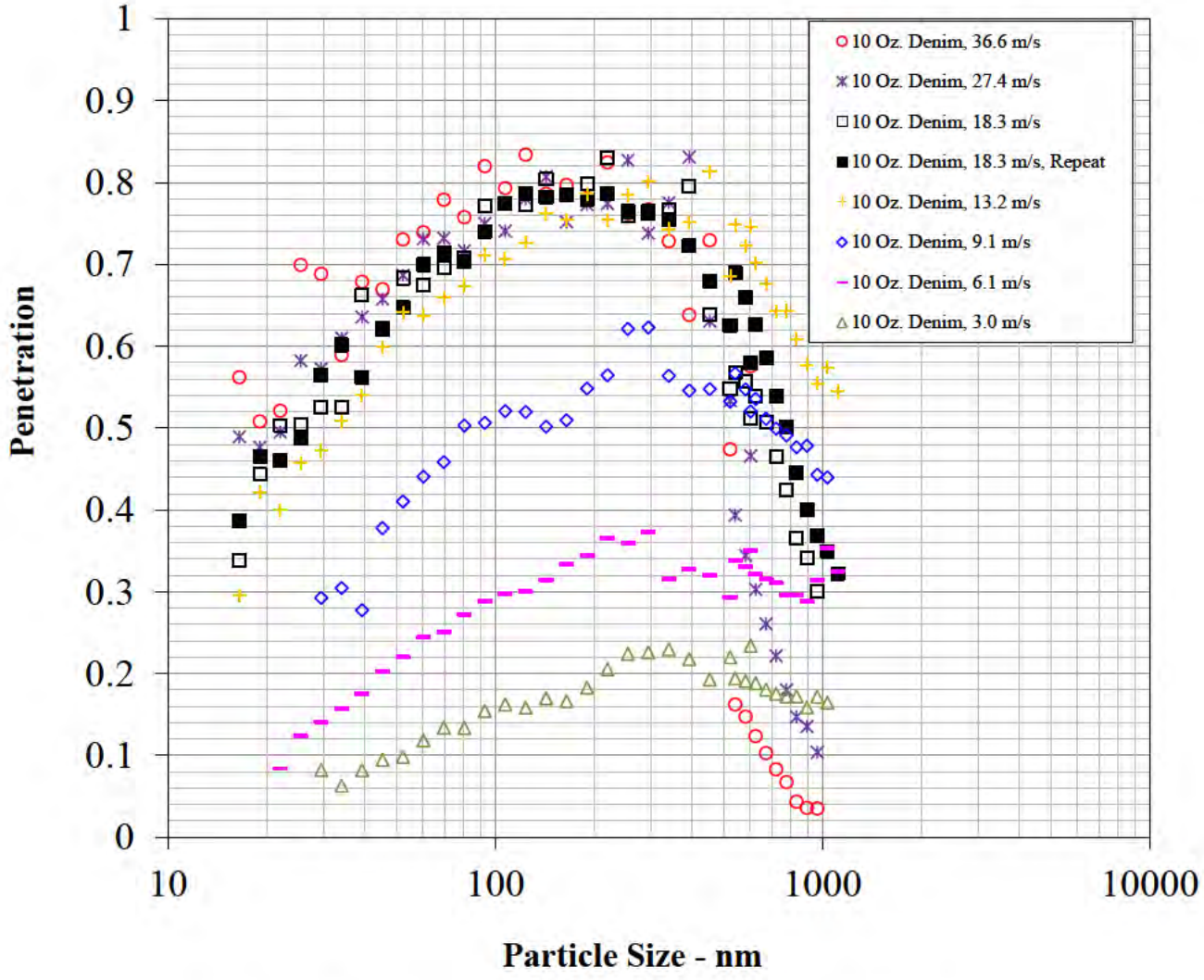

Figure A-25: Penetration Data for 10 oz Denim at $\psi = 0$ deg

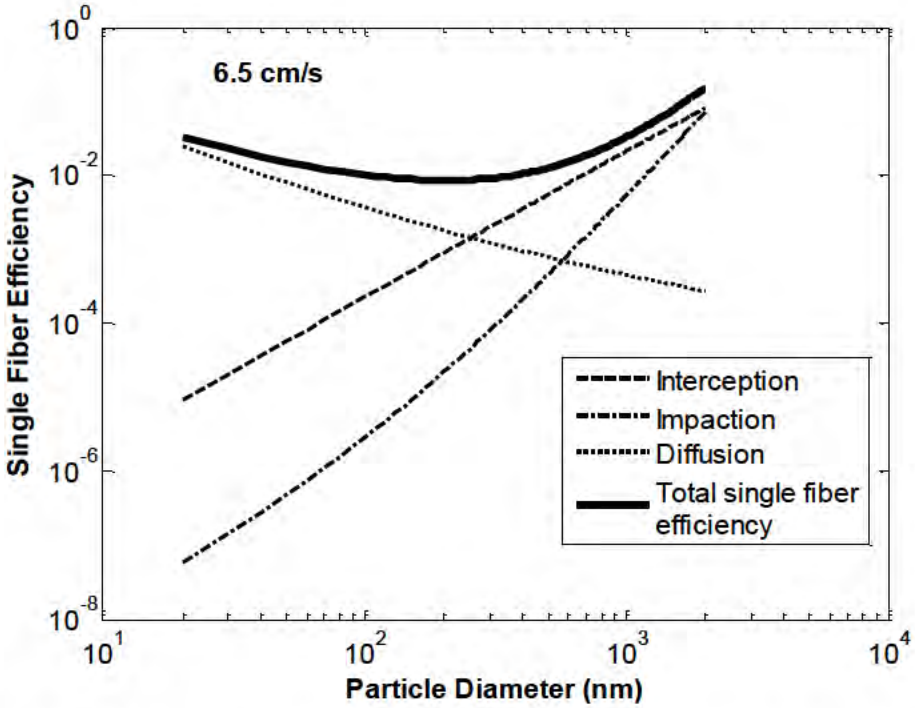

Figure A-26: Contribution of Filtration Mechanisms for 6.5 cm/sec Face Velocity (from reference 5)

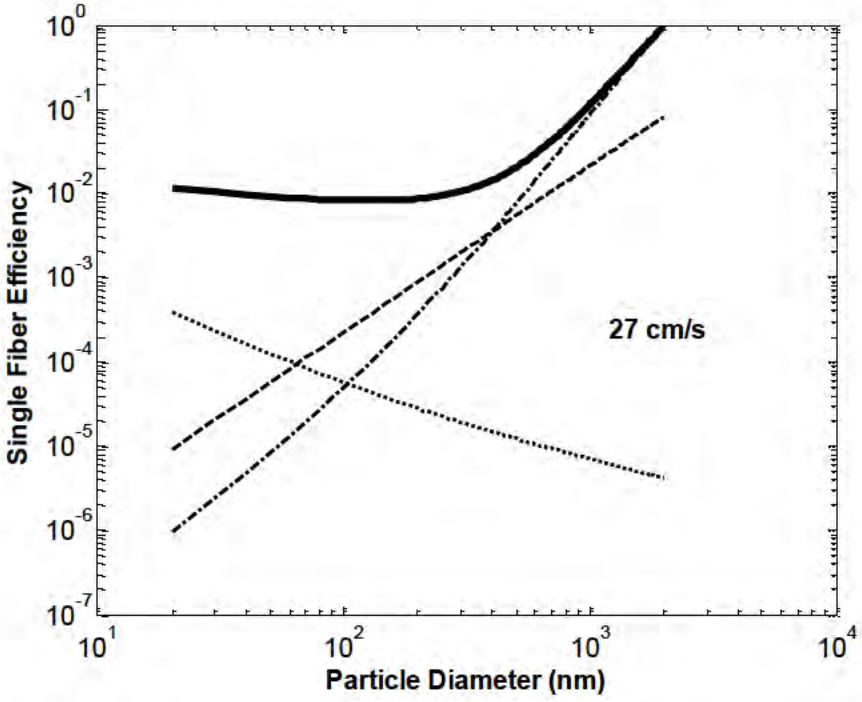

Figure A-27: Contribution of Filtration Mechanisms for 27 cm/sec Face Velocity

(from reference 5)

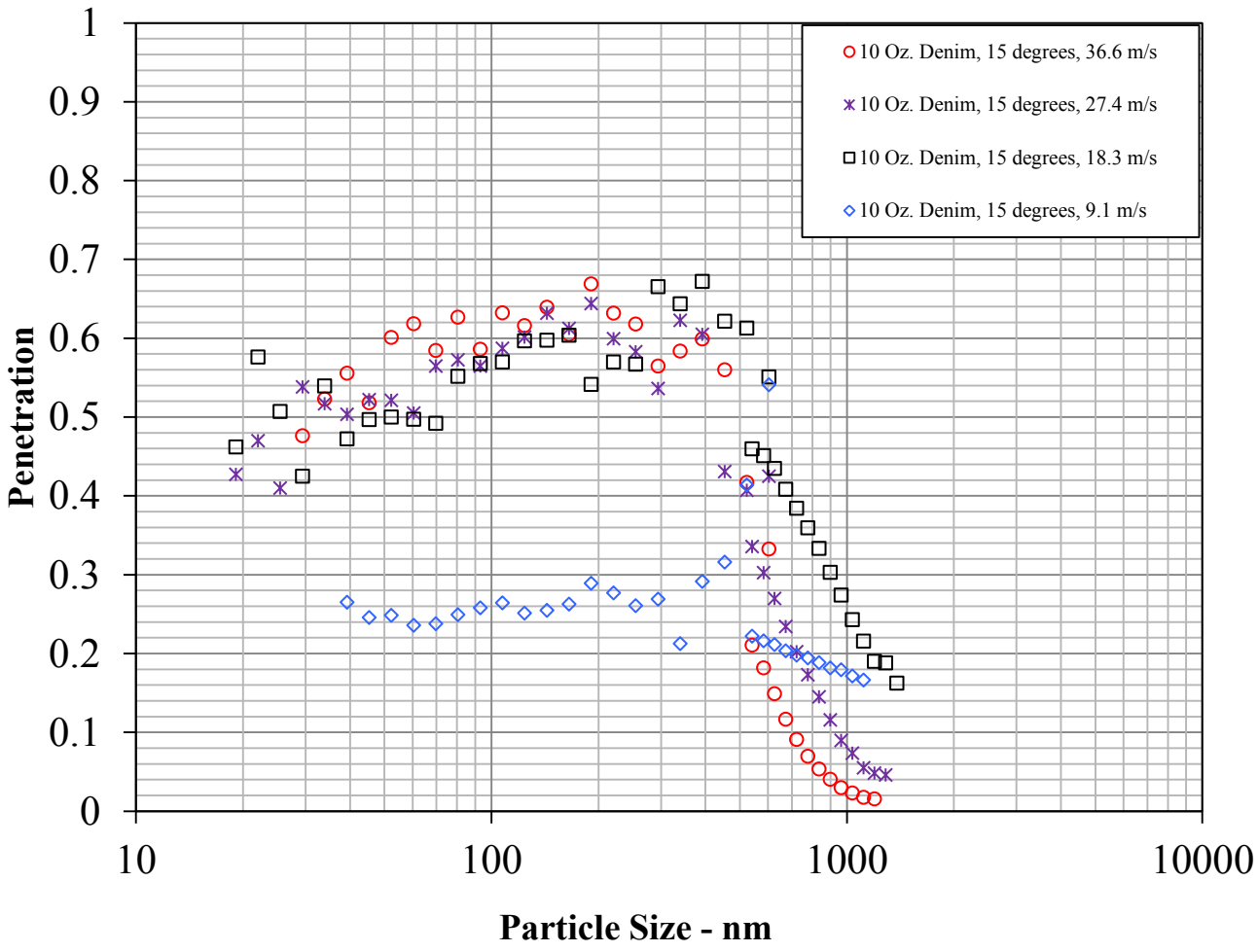

Figure A-28: Penetration Data for 10 oz. Denim at ψ = 15 deg

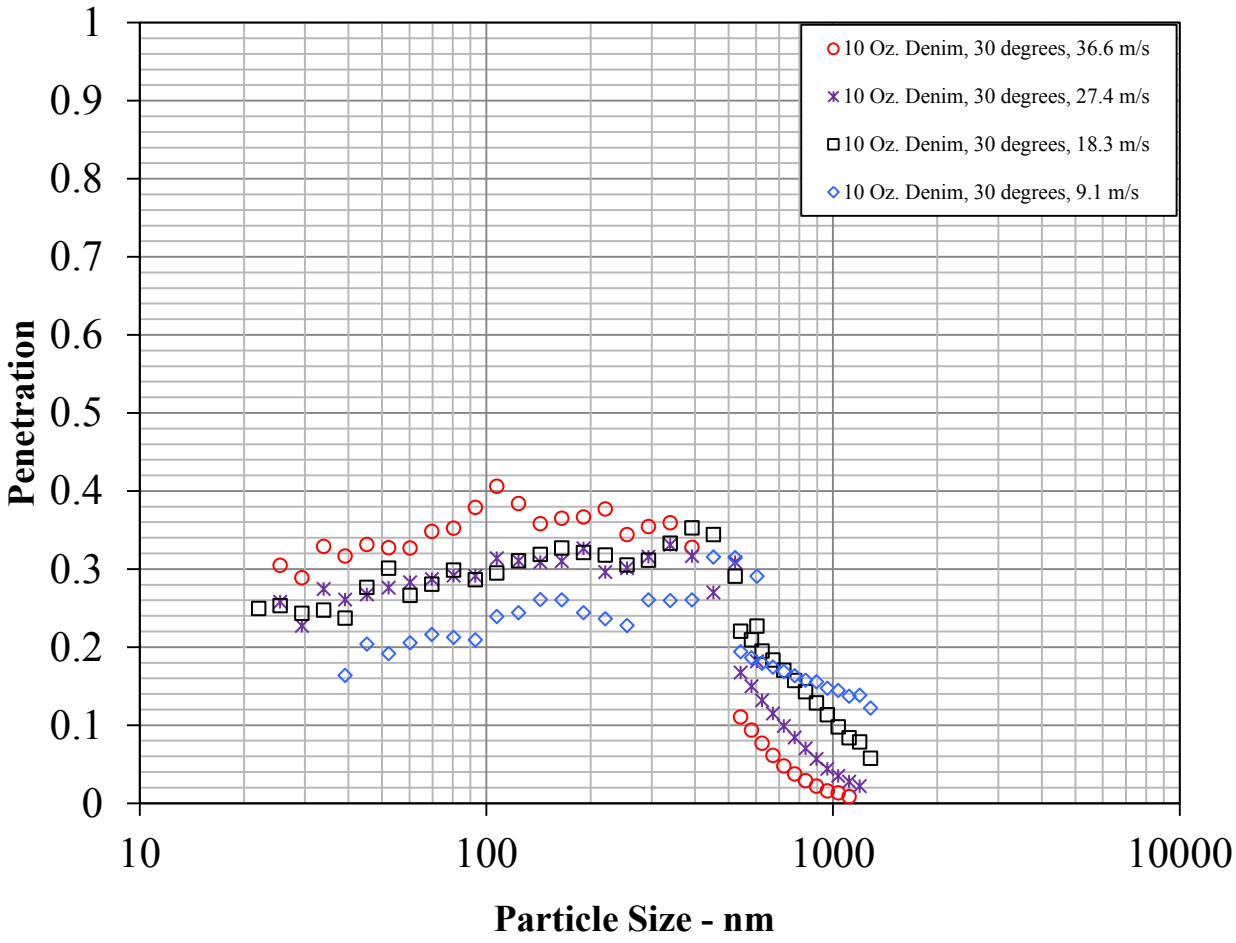

Figure A-29: Penetration Data for 10 oz. Denim at ψ = 30 deg

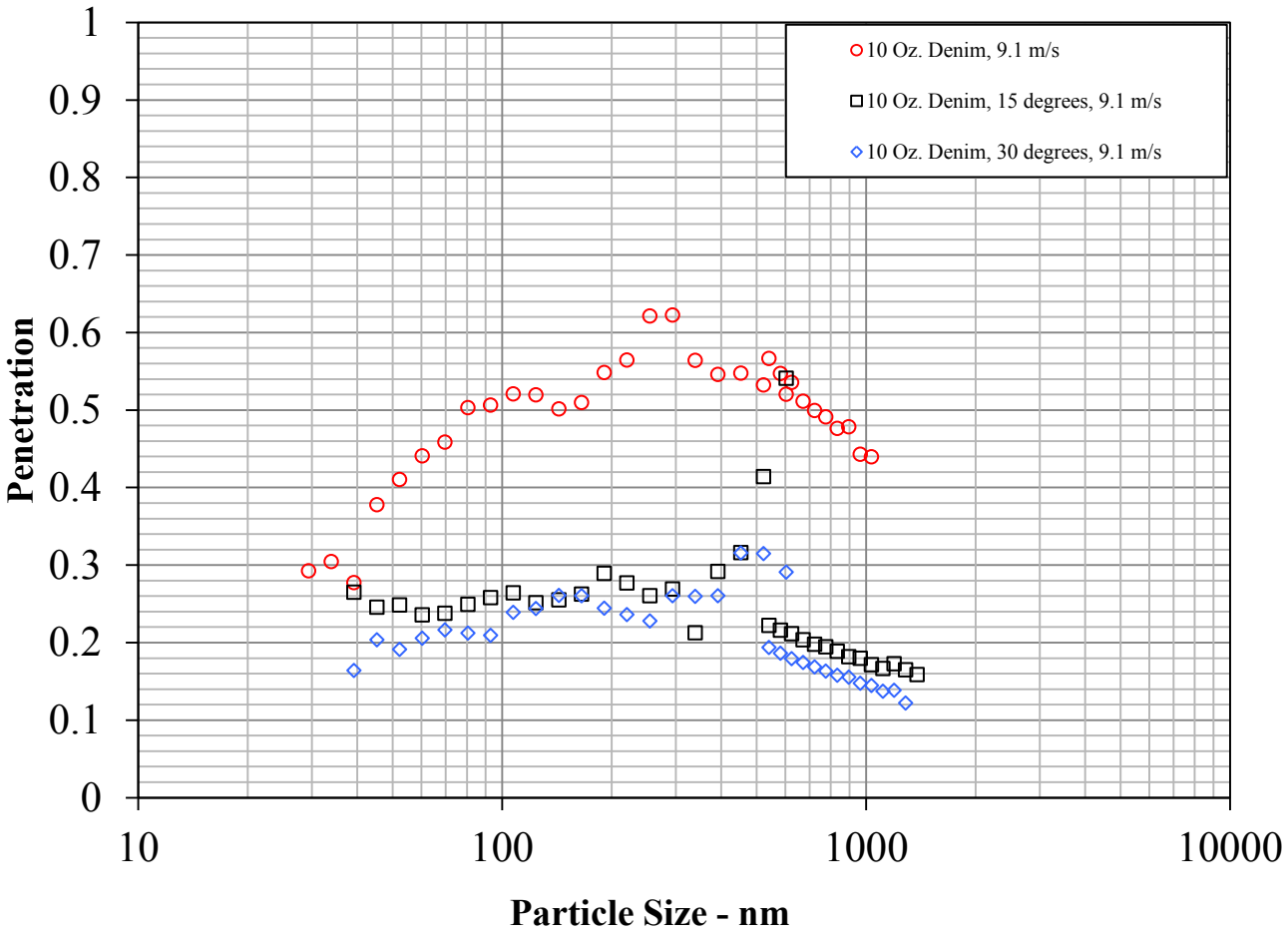

Figure A-30: Penetration Variation with Azimuth at Ambient Velocity = 9.1 m/sec

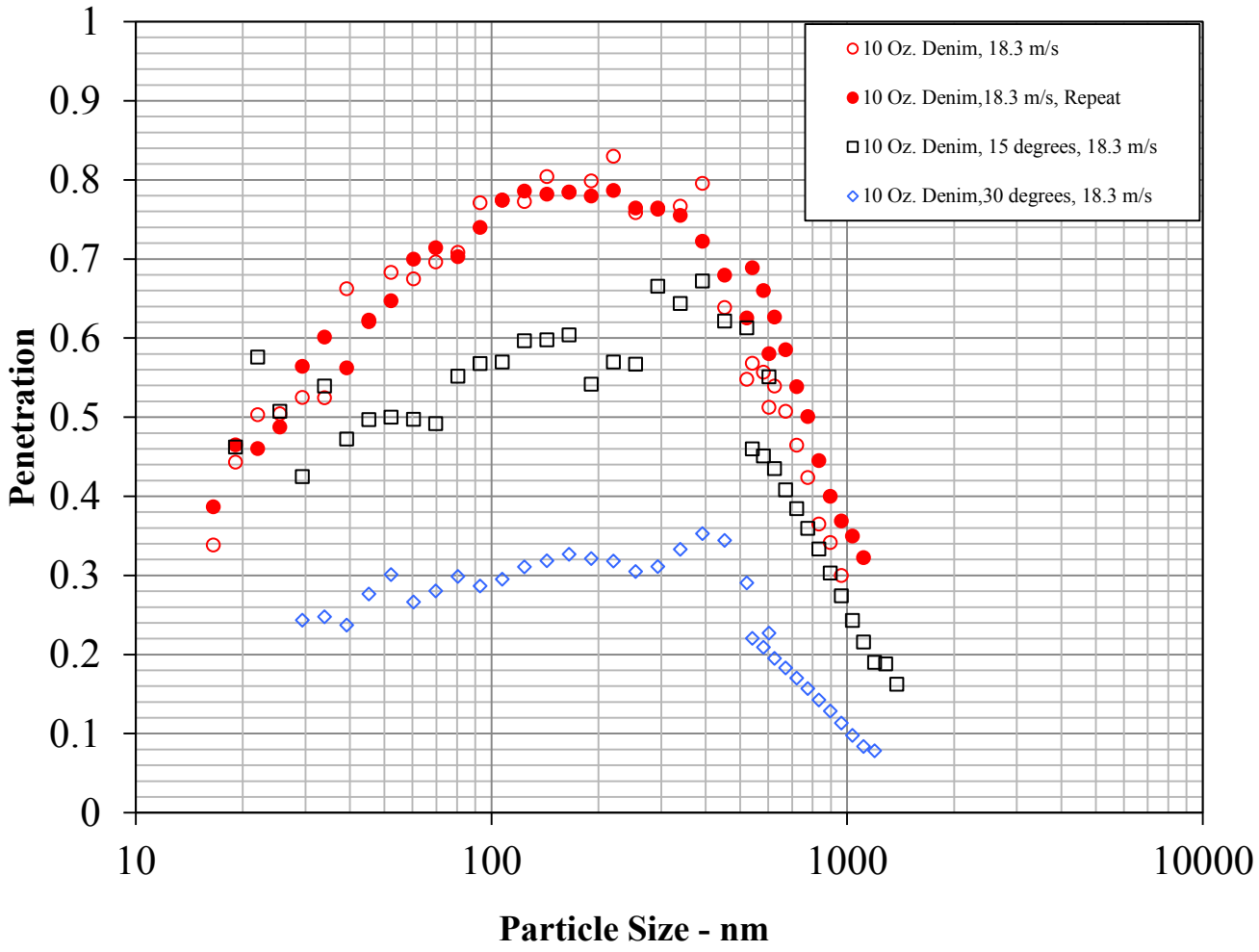

Figure A-31: Penetration Variation with Azimuth at Ambient Velocity = 18.3 m/sec

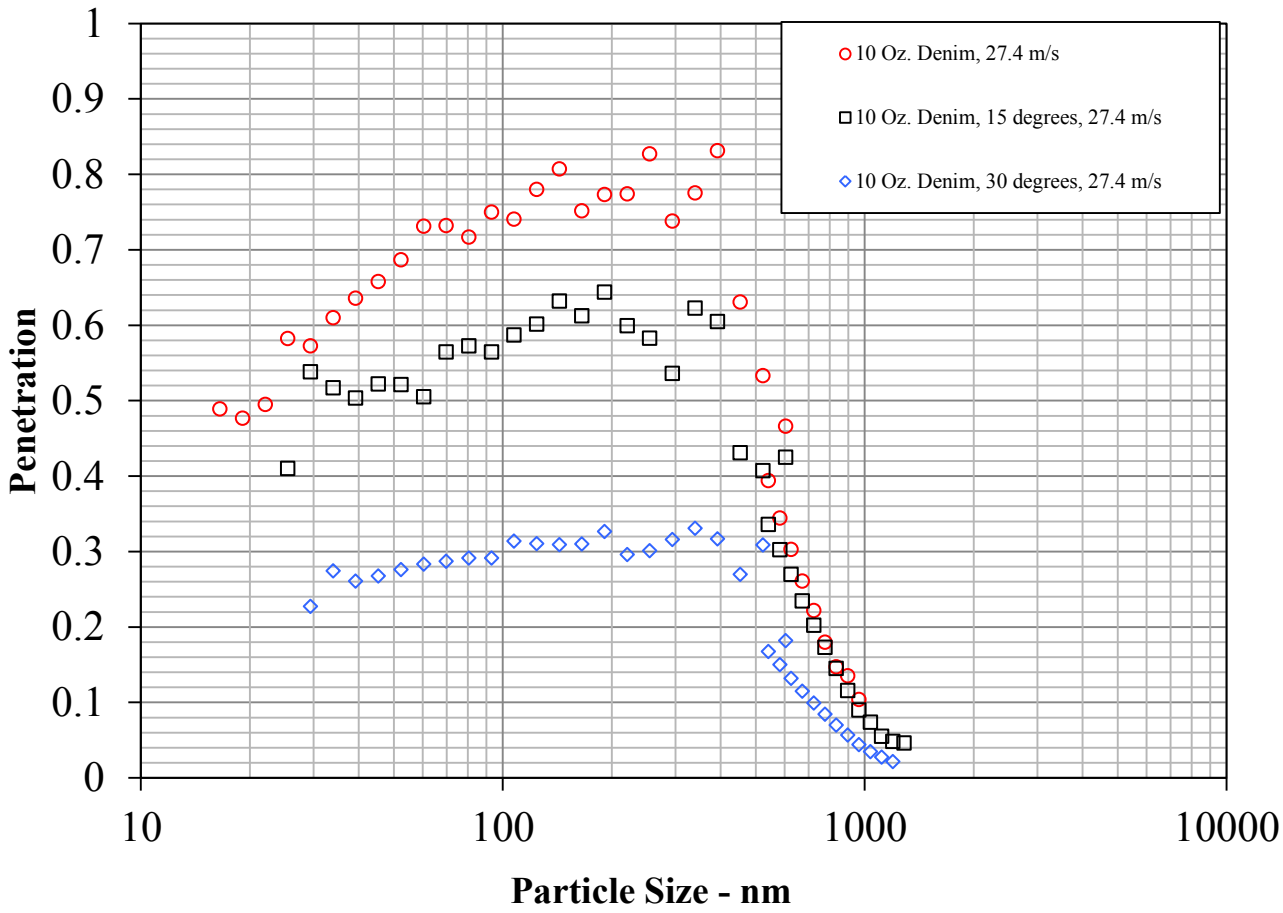

Figure A-32: Penetration Variation with Azimuth at Ambient Velocity = 27.4 m/sec

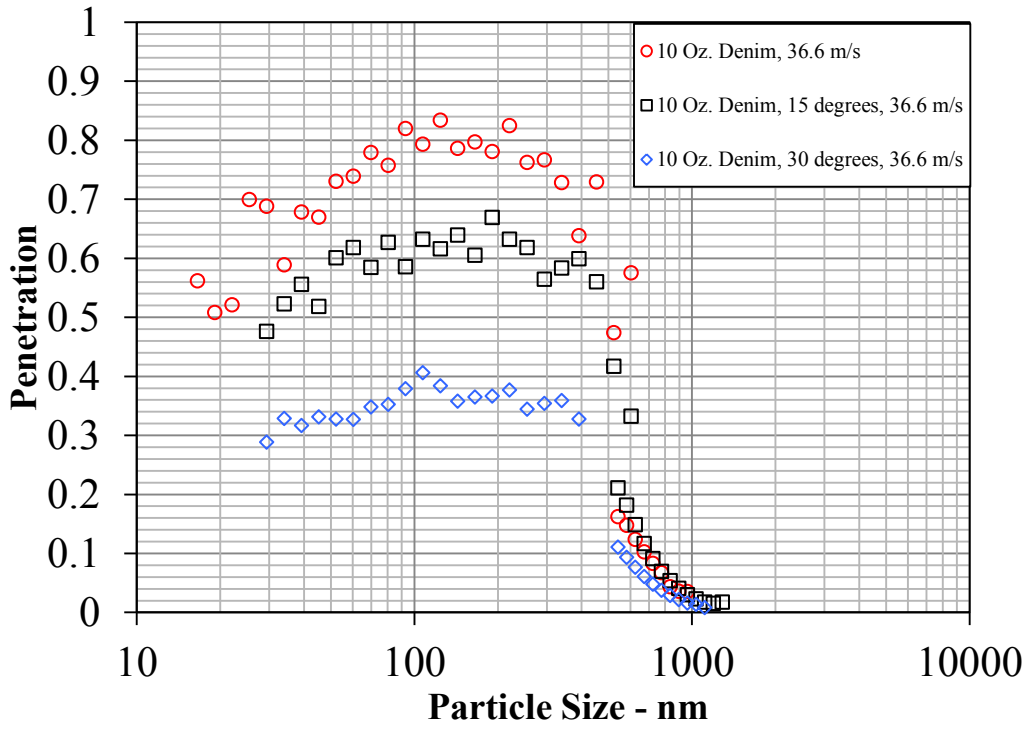

Figure A-33: Penetration Variation with Azimuth at Ambient Velocity = 36.6 m/sec

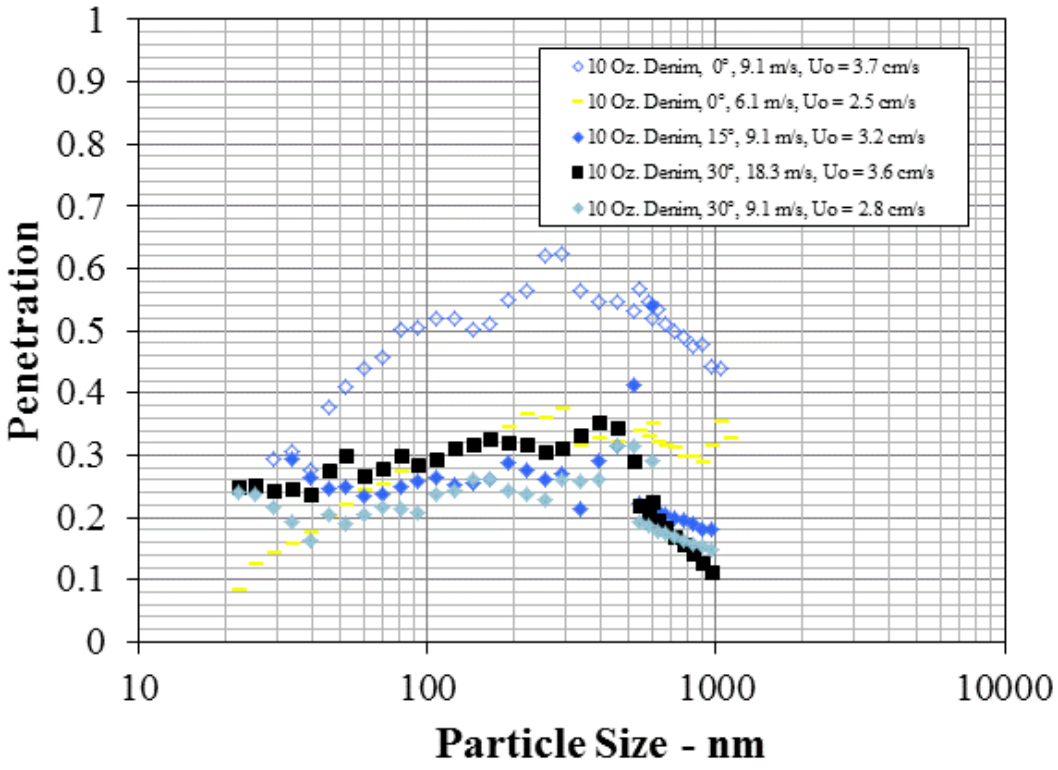

Figure A-34: Penetration Variation for U_o < 6 cm/sec

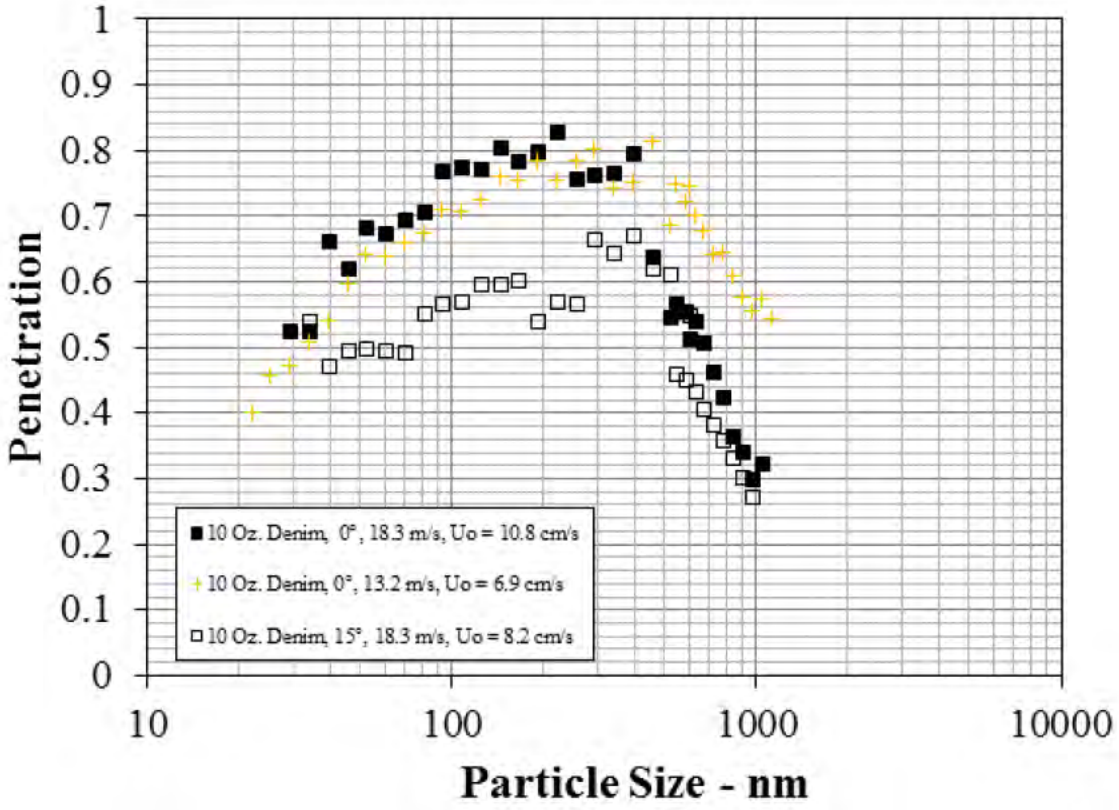

Figure A-35: Penetration Variation for 10 cm/sec > U_o > 6 cm/sec

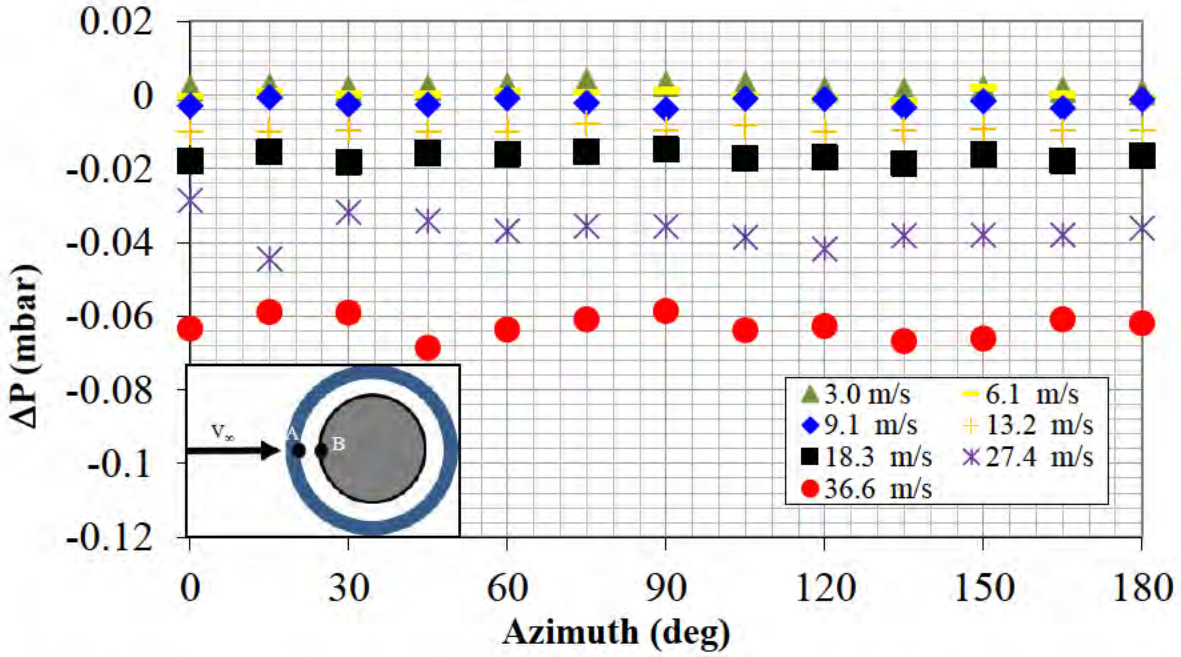

Figure A-36: Difference between Leeward Fabric Pressure and Corresponding Inner Cylinder Pressure Tap for 10 oz Denim Sleeve with Screen for Various Yaw Angles

APPENDIX B
TABLES

Table B-1: Instrumentation Settings

SMPS:	
Charge Correction	On
t_d (Delay Time)	3.3 s
Impactor	0.0457 cm
DMA	3081
CPC Model	3025A
CPC Flow	Low
Up scan	120 s
Down Scan	15 s
Sheath Flow	3 lpm
Aerosol Flow	0.3 lpm
Low Voltage	10 V
High Voltage	9630 V
Size Range	14.3 nm to 673 nm
t_f	7.4 s
D50	678 nm
APS:	
Dilution/Efficiency File	00100to1.e20
Particle Density (DOS)	0.914 g/cc
Stokes Correction	On
Channel	<0.523 to 20.535 micron
Sample Time	120 s
Summation	Channel and Raw data

Table B-2: Fabric Permeability Data

Material	Average Permeability (cm/sec)	Standard Deviation (cm/sec)	Number of Samples
10 oz Denim	3.1259	0.1697	26
A30	7.6193	0.6498	18
A30 + 10 oz Denim	2.5212	0.1731	15
Donaldson Dura-Life	10.0008	0.4479	14
Cotton Twill	8.4824	1.4392	16
Donaldson PTFE	5.0336	NA	1

Table B-3: ΔP_{max} Values for Figure A-18

	NAVAIR							Reference 16
V_∞ (m/sec)	3.0	6.1	9.1	13.2	18.3	27.4	36.6	4.500
ΔP_{max}	0.072	0.304	0.676	1.677	2.922	6.474	11.097	0.224

THIS PAGE INTENTIONALLY LEFT BLANK

DISTRIBUTION:

NAVAIRSYSCOM (4.3.2.1/Ghee), Bldg. 2187, Room 1320 48110 Shaw Road, Patuxent River, MD 20670-1906	(10)
Defense Threat Reduction Agency, JSTO CB/CBT 8725 John J. Kingman Road, Ft. Belvoir, VA 22060-6201 charles.bass@dtra.mil	(5)
US Army NSRDEC, RDNS-WSC-C (S. F. Zopf) 15 Kansas Street, Bldg. 4, Room D114, Natick, MA 01760 stephanie.f.zopf.civ@mail.mil	(3)
CLARKSON UNIVERSITY Mechanical Engineering Department 8 Clarkson Ave., Potsdam, NY 13699 sdhaniyala@clarkson.edu	(1)
NAVAIRSYSCOM (AIR-5.1V), Bldg. 304, Room 106A 22541 Millstone Road, Patuxent River, MD 20670-1606	(1)
NAVAIRSYSCOM (AIR-5.1), Bldg. 304, Room 100 22541 Millstone Road, Patuxent River, MD 20670-1606	(1)
NAVTESTWINGLANT (55TW01A), Bldg. 304, Room 200 22541 Millstone Road, Patuxent River, MD 20670-1606	(1)
NAVAIRSYSCOM (AIR-4.0T), Bldg. 407, Room 116 22269 Cedar Point Road, Patuxent River, MD 20670-1120	(1)
DTIC 8725 John J. Kingman Road, Suite 0944, Ft. Belvoir, VA 22060-6218	(1)